Tropical Cyclone Momentum and Energy Fluxes

by

William Douglas Ramstrom

Bachelor of Science in Computer Science and Engineering (1990),
Massachusetts Institute of Technology

Submitted to the Department of Earth, Atmospheric, and Planetary Science
in partial fulfillment of the requirements for the degree of

Master of Science

at the

MASSACHUSETTS INSTITUTE OF TECHNOLOGY

June 2001

Author .....
Department of Earth, Atmospheric, and Planetary Science
May 24, 2001

Certified by .....
Kerry A. Emanuel
Professor, Program in Atmospheres, Oceans and Climate
Thesis Supervisor

Accepted by .....
Ronald G. Prinn
Department Head, Department of Earth, Atmospheric and Planetary Sciences

Tropical Cyclone Momentum and Energy Fluxes

by

William Douglas Ramstrom

Submitted to the Department of Earth, Atmospheric, and Planetary Science
on May 24, 2001, in partial fulfillment of the
requirements for the degree of
Master of Science

Abstract

Many modeling studies of tropical cyclones use the bulk aerodynamic formulae to determine angular momentum and enthalpy fluxes at the sea surface. These results show that the intensification of a hurricane is very sensitive to the values of the coefficients defined in these formulae (Emanuel, 1995). Using these formulae allows the model to make bulk estimates of these fluxes as a function of wind speed, without having to consider the full complexity of the physics of the air-sea interface. Generally, a complete treatment of fluxes would require modeling a number of small-scale physical processes, e.g. wave field response to the duration and fetch of the wind, sea spray processes, and convective stability of the boundary layer.

The coefficients to these equations, C_d and C_k, have been empirically determined in previous studies, either by direct measurements on platforms and ships (Large and Pond, 1981), or by budget analyses from airborne data. However, these studies do not provide results for the high winds speeds encountered in strong hurricanes. Previous work has suggested that the coefficients do not remain constant, but rather are a function of wind speed. Producing values for these coefficients at high wind speeds will improve the accuracy of the numerical models.

Recent advances in dropsonde technology (Hock and Franklin, 1999) provide improved range and accuracy from earlier methods, with reliable measurements of wind and thermodynamic variables down to within 10m of the surface. Three cases of strong hurricanes have been selected for this study, allowing analysis of these coefficients for conditions with up to 65 ms^{-1} surface winds. The values of the drag coefficient, C_d, are demonstrated to reach a maximum value at about hurricane force, then maintain that value with higher wind speeds. The values of C_k, the heat flux coefficient, do not show variation with wind speed. These coefficients are calculated both at the standard 10m, so that they may be compared with existing literature, and at the top of the boundary layer, so that models which do not explicitly resolve the physics of the boundary layer may nonetheless make use of this data.

The budget calculations in this study have shown that the 10m drag coefficient has a value of 0.0026 to 0.0030 for wind speeds in the 40-60 ms^{-1} range. Eddy fluxes of total energy and entropy are also shown to be significant. With this effect added, budget calculations have shown that the 10m enthalpy transfer coefficient ranges from 0.0029 to 0.0036 under these conditions for Floyd and Georges. Thus, the ratio of C_k/C_d is slightly larger than 1.0. At the gradient wind level, C_d is 0.0019 ± 0.0010 and C_k is approximately 0.0018.

Thesis Supervisor: Kerry A. Emanuel
Title: Professor, Program in Atmospheres, Oceans and Climate

Contents

List of Figures

List of Tables

Chapter 1

Introduction

A hurricane can be thought of as a heat engine which derives its energy from the thermodynamic disequilibrium between the tropical atmosphere and oceans. Heat is input at the surface by sensible and latent heat fluxes, aided by the strong winds. Convective updrafts then transport this heat through the troposphere, and it is then exported at the temperature of the tropopause.

The turbulent processes that enable the flux of momentum and enthalpy at the sea surface can be idealized using bulk formulas. This allows a description of the magnitude of the flux based on observable features of the boundary layer, without resorting to a full description of the small-scale eddy field. Instead, the momentum and enthalpy fluxes are represented by functions of the 10m wind speed and non-dimensional exchange coefficients. For enthalpy, the flux is also modeled as a function of the enthalpy difference between the sea surface value and the value at 10m. For the angular momentum budget, the sea surface is idealized as having no horizontal motion. When compared to the eyewall wind velocities of > 30 ms^{-1}, a current of a few ms^{-1} can be neglected. The 10m wind values are chosen because this is the standard used in the literature for these calculations. Given that the soundings provide winds at all levels, this choice is somewhat arbitrary, but it allows comparison with previously determined values for the exchange coefficients. Since the wind increases with height in the hurricane boundary layer, it is clear that the coefficients are specific to the altitude of the wind used. Versions of the coefficients will also be calculated at the top of the boundary layer, where winds are in gradient balance.

Some work has been done measuring these coefficients under low wind speeds, but it is difficult to measure them under the extreme conditions of a hurricane. In general, direct measurements require a stable platform at some elevation above the sea surface and a continuous period of observations. In hurricanes, instead, more indirect approaches must be used, due to the difficulty of making such fixed-site observations. These are generally based on analyzing a budget of angular momentum and total energy in the storm and using the assumption that the residual fluxes must be across the sea surface.

The drag coefficient, C_d, can be estimated by considering a budget of angular momentum. The definition of angular momentum, M, is given in equation 1.1, where V is the tangential wind, r is the radius from the center of the storm, and f is the Coriolis parameter.

$$M = Vr + \frac{fr^2}{2} \tag{1.1}$$

The aerodynamic flux formula for angular momentum is then expressed in equation 1.2, where τ_θ is the shearing stress in the $\Theta - Z$ plane, ρ_0 is the density of the air at the surface, C_d is the momentum flux coefficient, V is the tangential (azimuthal) wind at 10m, and $|\mathbf{V}|$ is the magnitude of the wind speed at 10m.

$$\tau_\theta = \rho_0 C_d V|\mathbf{V}| \tag{1.2}$$

The flux of enthalpy serves as the source of energy for the development and maintenance of the hurricane. The total energy is a similar quantity, that also includes the effect of gravity and the kinetic energy of the wind. Enthalpy, k, is defined in 1.3, where k is the enthalpy, c_{pd} is the heat capacity at constant pressure for dry air, q_t is the total specific water content (mass of all phases of water/mass of (moist) air), c_l is the heat capacity of liquid water, T_0 is a reference temperature, L_v is the latent heat of vaporization of water (a calculated value), and q is the specific humidity (mass of water vapor/mass of (moist air)),

$$k = (c_{pd}(1 - q_t) + c_l q_t)(T - T_0) + L_v q \tag{1.3}$$

Total energy is defined in equation 1.4, where g is the gravitational constant, z is the geopotential height, and $|\mathbf{V}|$ is the wind speed. For calculations of E of the sea surface, a

value of $|\mathbf{V}|$ which is the gradient wind at that radius will be used.

$$E = (c_{pd}(1 - q_t) + c_l q_t)(T - T_0) + L_v q + gz + \frac{|\mathbf{V}|^2}{2} \tag{1.4}$$

The flux of enthalpy across the sea surface is the only source of total energy in this system; away from the surface, total energy is approximately conserved. The aerodynamic flux formula for enthalpy is shown in 1.5, where F_k is the air-sea flux of enthalpy, C_k is the enthalpy flux coefficient, k_s^* is the saturation enthalpy of the sea surface, and k is the enthalpy of the atmosphere, and $|\mathbf{V}|$ is the magnitude of the wind speed at 10m. The saturation enthalpy is just the enthalpy calculated using the sea surface temperature and a relative humidity of 100%.

$$F_k = \rho_0 |V| C_k (k_s^* - k) \tag{1.5}$$

While these coefficients have been extensively estimated in laboratory and field studies, this has only been for relatively light wind speeds (up to about 20 ms^{-1}); Large and Pond (1981). A few observational studies have provided values for these coefficients by estimating values from budget residuals, rather than direct observation, and they do show that drag coefficients continue to increase as windspeeds approach hurricane force (33 ms^{-1}) (Hawkins and Rubsam, 1968).

Many models of tropical cyclones make use of bulk aerodynamic formulae for parameterizing air-sea fluxes of heat, moisture, and momentum. Thus, it would be useful to extend the calculations to strong hurricane conditions (> 40 ms^{-1}) to determine whether the same relationships hold. It has been shown (Emanuel, 1995) that models are quite sensitive to the ratio of these values, so determining accurate values for the full range of hurricane conditions would be a great help in improving the accuracy of these models.

This study will make use of the GPS dropsonde and flight-level data sets gathered by the Hurricane Research Division (HRD) to see whether the observed fluxes of enthalpy and angular momentum can be estimated using the bulk aerodynamic formulae. The greatly increased vertical resolution and consistent collection of data down to very close to the sea surface is an important improvement over what was previously available. In addition,

new technology in sonde tracking and improvements to instruments aboard the sonde will also provide more accurate data. The low-level observations are crucially important in this effort, as the wind, moisture, and temperature profiles can vary strongly in the frictional layer near the surface, so interpolation from higher levels may not be accurate.

In particular, several cases of very strong hurricanes (Floyd, Georges, and Mitch) will be examined, as these storms had very high surface wind speeds (> 60 ms^{-1}) as well as good dropsonde coverage of the important eyewall region. Expendable bathythermographs were deployed for all of these storms; their data will be used to assess the temperature structure of the upper levels of the ocean under the hurricane eyewall and inflow regions.

1.1 Data Sources

A number of sources of data are used for this study. GPS-dropsondes from NOAA and Air Force Reserve missions provide the details of the vertical structure of the atmosphere for the systems. In addition, flight level data collected on-board the reconnaissance aircraft were also incorporated into the analysis. Best track data, tabulated by the Hurricane Research Division (HRD) using satellite, radar, and reconnaissance information are included in the flight level dataset. This best track data, though, have some uncertainty associated with it; in fact at some times, more than one center location is represented in this data. This is due to the algorithms for calculating the center, which are based on observations at a given pressure level.

For the 1998 and 1999 Atlantic hurricane seasons, vertical sounding profiles using NCAR GPS dropsondes were gathered. These sondes give detailed wind, pressure, temperature, and humidity measurements at high resolution throughout their descent (Hock and Franklin, 1999). Of particular note for this work, high resolution of observations is available down to the surface, with data gathered at about every 5m in the vertical. Wind data is also much improved by using this new sonde. The older Omega sondes had vertical resolution of 150m, and could not yield winds below 400m. The GPS sondes give wind readings at about 5m increments in the vertical, down to within 10m of the sea surface.

Dual, heated humidity sensors are used to give accurate moisture readings; one is heated

Pressure	1.0 mb
Temperature	0.2^oC
Humidity	< 5 %
Wind	0.5-2.0 ms^{-1}

Table 1.1: Measurements errors for GPS dropsondes

while the other is measuring humidity values, then the pattern is reversed. From Hock and Franklin, 1999, typical measurement errors are given in Table 1.1. Wetting of probes by spray in the lowest levels may also introduce errors; however examination of the temperature and humidity profiles in the lowest tens of meters did not show this effect.

Chapter 2

Previous Work

A number of approaches have been tried for estimating the transfer coefficients of enthalpy (latent and sensible heat) and momentum over the ocean. In general, all results have shown that C_d increases with wind speed, while C_k remains approximately constant with wind speed (though it is affected by vertical stability). The variations of C_d with windspeed are generally accepted to be due to the interaction with the wave field; a few studies have shown that a better relationship can be derived by fitting C_d as a function of the sea state (wave age) rather than to wind speed. Many of the observations have been made in conditions that are not identical to hurricane cases; either at mid-latitudes over cool water or over the tropics but in light wind regimes. Nevertheless, these studies provide a good starting point for understanding how the transfer coefficients vary with wind speed and other factors.

2.1 Platform Studies

Measurements of wind stress and heat flux have been performed at various locations around the world using ocean platforms or stations located on low-lying islands. These have all been in mid-latitude zones. Geernaert et al. (1987) made measurements on a platform in the North Sea over a range of windspeeds from 5-30 ms^{-1}. An important finding of this study was that the wind stress coefficient could be better modeled as a function of wave age than of wind speed. Wave age is defined as $\frac{C_o}{u_*}$, where C_o is the phase speed of the dominant long wave, and u_* is the friction velocity; small values of wave age correspond to

growing waves. On the other hand, they found no dependence of the heat flux coefficient on wind speed or wave age; values for C_h were $0.705 \cdot 10^{-3}$, with a standard deviation of $0.275 \cdot 10^{-3}$.

Large and Pond, (1981) made observations in a variety of deep-water environments, including aboard ships on the open ocean. Observations were also taken on a platform off of Halifax, NS. They found a formula for the drag coefficient based on windspeed as follows: $10^3 C_d = 0.49 + 0.065 U_{10}$ for winds of 11 m/s to 25 m/s. They note that C_d is smaller during increasing winds, and larger during falling winds or after a wind shift. This supports the ideas about wave age presented in Geernaert et al. (1987).

Large and Pond, (1982) documented findings for heat fluxes based on the same observations as in the previous case for momentum. They found a sensible heat flux $C_h = 1.13 \cdot 10^{-3}$ for unstable conditions over a range of 4-25 m/s, and a latent heat flux $C_e = 1.15 \cdot 10^{-3}$ for unstable conditions over a range of 4-14 m/s. Neither showed a dependance on wind speed.

Smith and Banke, (1980) made observations on a tower at a flat, exposed location at the tip of Sable Island, NS. Only cases with a flow off the ocean were used. They found a relation for the drag coefficient as follows: $10^3 C_d = 0.63 + 0.066 U_{10} \pm 0.23$ for winds of 3 m/s to 21 m/s.

Smith, 1980 made additional calculations based on observations from a platform offshore of Nova Scotia. Observations were taken during the fall through spring seasons, but ended when the moorings collapsed on February 7, 1978. The coefficient of sensible heat flux, C_h, was found to be $1.10 \cdot 10^{-3}$ for unstable conditions; this result does not have a strong wind speed dependence over the range 6-22 m/s. The relation for the drag coefficient is $10^3 C_d = 0.61 + 0.063 U_{10} \pm 0.23$ for winds of 6 m/s to 22 m/s.

2.2 TOGA COARE Studies

Budgets of momentum and heat flux were calculated using the data from TOGA-COARE in Fairall et al. (1996). A windspeed range of 0.5 to 10 ms^{-1} was observed during the time of the measurements. This study found a heat transfer coefficient in neutral conditions of $1.1 \cdot 10^{-3}$. Several secondary effects of the fluxes are mentioned in this paper; these are

evaluated to see whether they are important in the hurricane cases. Fairall et al. (1996) noted that the saturation mixing ratio over the ocean surface will be slightly lower than the ideal case over pure water due to salinity effects. This is expressed as $q_s = 0.98 q_{sst}(T_s)$, where q_s is the saturated mixing ratio over the ocean, and $q_{sst}(T_s)$ is the saturated mixing ratio over pure water at the sea surface temperature. This salinity effect should be small for the cases we will consider, especially when compared to the uncertainty in the measurements of SST, so these modifications are not included in our calculations.

2.3 Hurricane Data Studies

Hawkins and Rubsam (1968) attempted to estimate the angular momentum budget of a mature hurricane. The heat transfer coefficient was assumed to be equal to the momentum coefficient. That study used the data collected aboard reconnaissance aircraft to develop the budgets, thus they had data at only a few vertical levels. In order to composite the data, the storm was assumed to be symmetric about the eye, and calculations were performed in cylindrical coordinates. They noted that this method is very sensitive to the exact determination of the center of the storm, due to the decomposition of winds into radial and tangential components. At inner radii, a small change in the center location can cause a large change in the magnitude of the computed radial velocity.

Their results showed increasing values of the drag coefficient over the range of windspeeds examined, with a similar relation to windspeed as that found in Large and Pond (1981), though extended up to a maximum windspeed of 42 ms^{-1}, where C_d was 0.0036.

Chapter 3

Overview of Cases

3.1 Floyd

Hurricane Floyd was sampled on 13-14 September 1999 by two reconnaissance aircraft. At that time, Floyd was a category 4 hurricane located over the eastern Bahamas, moving westward, with maximum winds of 135 knots and a central pressure of 921 mb (Black, 1999). This was the maximum intensity of Floyd; wind and surface pressure measurements indicate that it was in a quasi-steady state during the time of this mission. A notable feature of Floyd is the presence of two concentric eyewalls, one with a radius of 20km, and another with a radius of 90km (Figure 3-1). There is good data coverage of both eyewalls for all quadrants. The presence of two eyewalls will be seen to give Floyd a velocity profile that drops off more slowly with radius than the two other cases. A reflection of the outer eyewall is seen in Figure 4-3, where upward vertical motion extends out to just past 100km from the center. Note the 'moat' of lower intensity radar returns between these two eyewalls, which leads to a structure of two updraft maxima at 20km and 90km. The first dropsonde was released at 1916Z on 13 September 1999, the last of the mission was released at 0004Z on 14 September 1999. Over the course of several passes through the storm, a total of 29 drops were performed in the outer regions of the storm, in both of the eyewalls, and in the eye.

A total of 8 expendable bathythermographs (AXBTs) were deployed over the same period, scattered around the immediate environment of the hurricane. Sea surface temper-

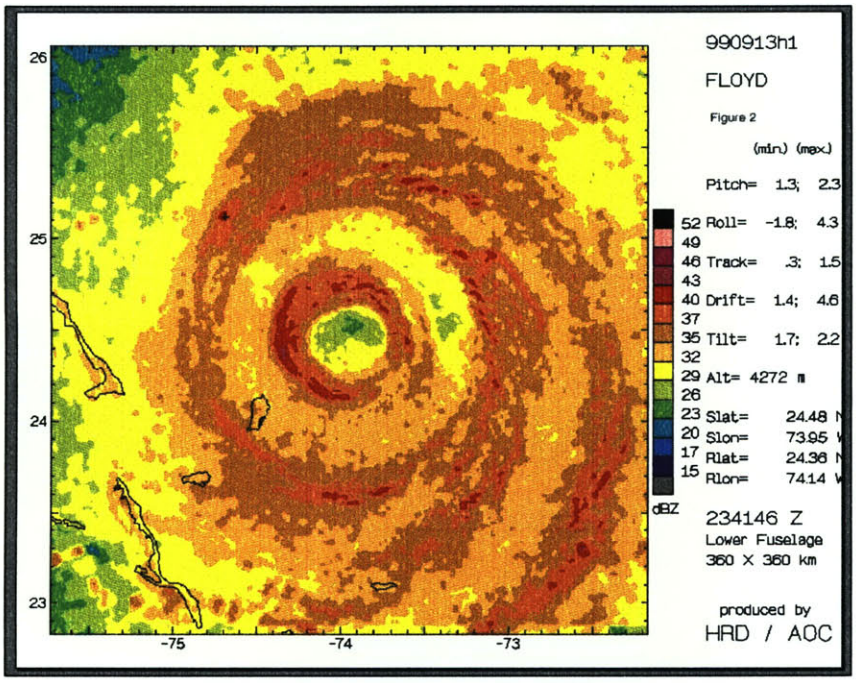

Figure 3-1: Floyd Radar Image 13 September 1999 2341Z

atures ranged from 26.05^oC to 28.64^oC. Water temperature readings down to 100m depth were returned by the AXBTs, showing the presence of a mixed layer ranging between 40m and 60m in depth.

3.2 Georges

Hurricane Georges was sampled on 19-20 September 1999, while it was east of the Lesser Antilles, moving westward. At this time, maximum surface wind speed were 125-130 knots, making it a category 4 hurricane, with a sea level pressure of 940 mb (Black, 1998). Radar data (Figure 3-2) shows a symmetric eyewall of radius 15km, with strong convection covering all sections except for the southern end. A large area of strong convection extends away from the eyewall, with some spiral bands embedded, especially towards the southwest. Three aircraft sampled Georges between 1756Z 19 September 1999, and 0146Z 20 September 1999. A total of 83 dropsondes were deployed at various ranges, though some were far from the storm center. Several AXBTs were deployed near Georges, reporting an average

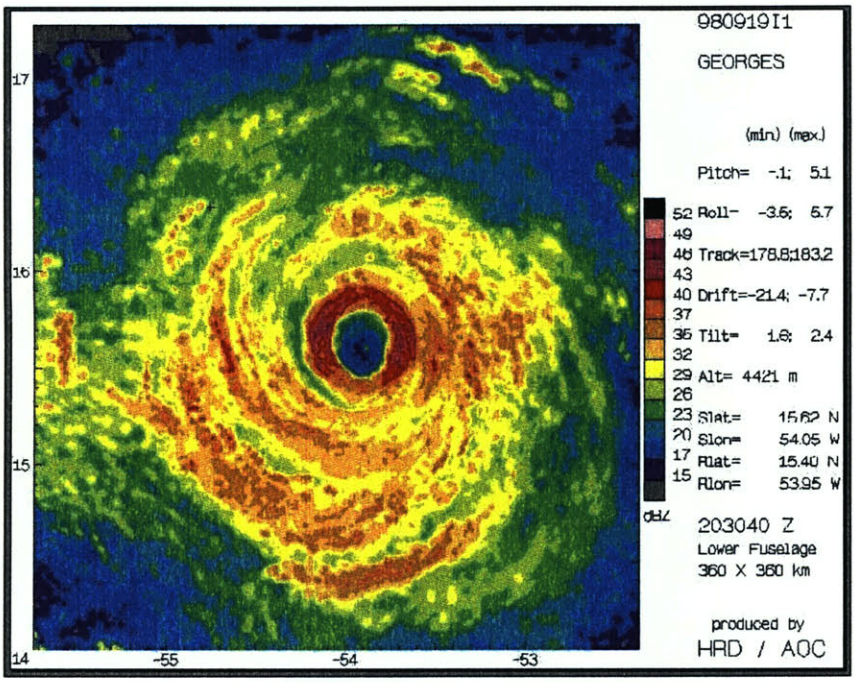

Figure 3-2: Georges Radar Image 19 September 1998 2030Z

surface temperature of 27.83^oC, with a range between 26.07^oC and 28.64^oC.

3.3 Mitch

Hurricane Mitch was sampled on 27 October 1998 by a single aircraft. At that time, it was located in Caribbean just offshore from Honduras. Mitch had attained its maximum strength the previous day, but remained at strong category 4 hurricane at the time of measurements, with estimated surface winds of 135-140kts and central pressure of 930mb. Several of the dropsondes, however, measured winds in excess of these values, with some values above $90ms^{-1}$. A number of the sondes failed to report measurements all the way to the surface, probably due to the extreme winds. Despite the strength of Mitch, the eyewall was asymmetrical, maintaining an elliptical shape, 30km across east-west, and 40 km across north-south, as shown in Figure 3-3. Convective elements formed in the southeast quadrant of the eyewall and rotated northward and dissipated (Black, 1998b). A number of other asymmetries were noted during the flight, making this case less well-suited for azimuthal

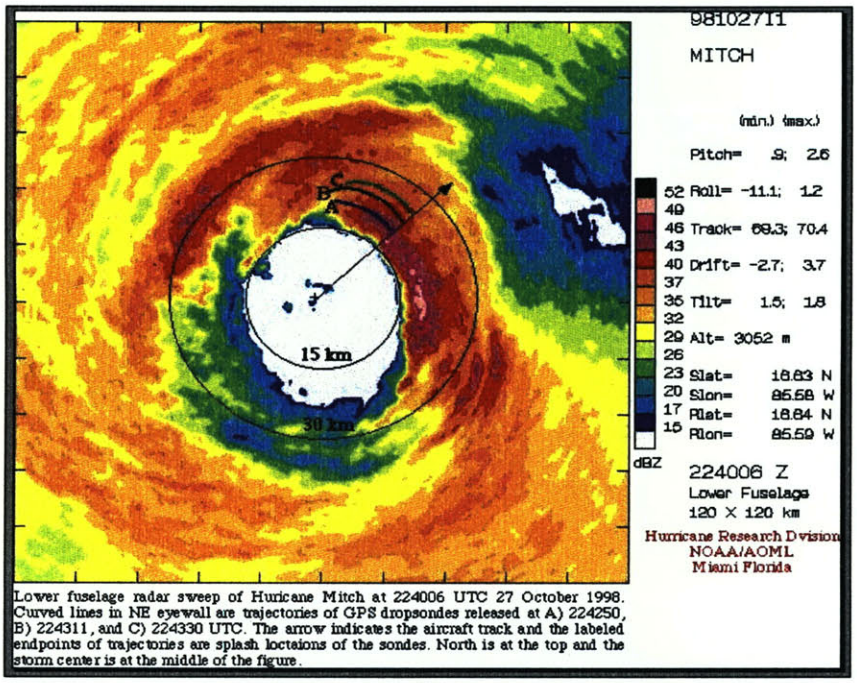

Figure 3-3: Mitch Radar Image 27 October 1998 2240Z

compositing than the previous cases. In addition, the storm moved erratically over the time of sampling, making the position and motion estimates more difficult and error-prone.

Six AXBTs successfully reported data, indicating sea surface temperatures of $28 - 29^{o}C$ (Black, 1998b).

Chapter 4

Data Analysis

4.1 Analytical Framework

4.1.1 Equations and Coefficients

The flight and sounding data are transformed into potential radius coordinates. The benefit of using this coordinate system is that it gives much higher resolution in areas of high winds, which is the area of greatest interest for this study. The potential radius, R, is defined in equation 4.1, where f is the Coriolis parameter, r is the physical radius, and V_t is the tangential wind.

$$\frac{1}{2}fR^2 = \frac{1}{2}fr^2 + V_t r \tag{4.1}$$

This coordinate system imposes the constraint that the flow should be inertially stable; i.e. r should increase with R. In evaluating a composite, this can be used to assess its validity; if r does not monotonically increase with R, we have an inertially unstable profile; if this is true, we most likely have a problem with the profile. In practice, a source of error is in selecting the center of the storm, such that a sounding in the eye with light winds is assigned a larger physical radius than a sounding in the eyewall with hurricane-force winds. Such a setup would cause the eyewall sounding to have a very large potential radius due to the strong tangential winds, while the eye sounding would have a small potential radius. Another cause is asymmetry of the storm, as the storm has been assumed to be

axisymmetric. If different quadrants of the storm are of differing strengths, then the radial profile will not be uniform.

Examination of the wind profiles in hurricanes shows that tangential winds drop off significantly in the boundary layer from the values observed above the boundary layer. This means that the angular momentum surfaces flare outwards near the ocean surface when considered in physical radius space. Thus, the radial winds are not perpendicular to these surfaces, and a component of the vertical motion also crosses them. In the boundary layer, where friction and turbulence induced by the surface are important, it is not clear that the system can adjust to be neutral to slantwise convection while being forced by turbulence. In order to simplify the form of the budget equations, a modified version of potential radius is used in the boundary layer, where the 1000-1200m mean value of tangential wind is used instead of the observed value. The boundary layer potential radius coordinate is defined in equation 4.2, where f is the Coriolis parameter, r is the physical radius, and $V_{gradient}$ is the tangential wind above the boundary layer. This produces a coordinate system that retains the useful scaling relationship of potential radius, such that the eye and inner eyewall have high resolution, but also has perpendicular and parallel alignment, respectively, to the radial and vertical winds. This means that the radial winds are perpendicular to the surfaces of R, rather than needing a transformation.

$$\frac{1}{2}fR^2 = \frac{1}{2}fr^2 + V_{gradient}r \tag{4.2}$$

A modified version of radial wind speed is defined in equation 4.3, which gives the displacement of a parcel in terms of potential radius instead of physical radius. This modified radial wind speed, $u' \equiv \frac{dR}{dt}$, is used to calculate advection of quantities where the radial variations are phrased in potential radius coordinates instead of physical coordinates, where the untransformed radial wind, u, is used.

$$u' = \frac{(fr + v_{grad})u}{fR - r\frac{\partial v_{grad}}{\partial R}} \tag{4.3}$$

4.1.2 Radial Compositing

Data from the flights and dropsondes are composited into a radially symmetric grid, with coordinates of potential radius in the radial direction and height in the vertical. Height was chosen for this work because the during times of interest the storms are over the sea, so we can use a lower surface of z=0.

A reasonable approximation of tropical cyclone structure is to assume radial symmetry about the eye of the storm. The most important benefit of this approach is that it gives good data resolution in the radial that would be lacking if we attempted to account for the three-dimensional structure. Axisymmetric models of hurricane behavior have long been used, e.g. (Ooyama, 1969), (Emanuel,1995), because the important dynamical properties of the storm, such as the eye, eyewall, and low-level inflow, can all be seen without resorting to a more complicated 3-dimensional model. There are effects which can only be seen using a full 3D model, such as beta gyres, but in general their influence on wind speed and convergence is small. These effects are more often studied to help determine storm motion, which cannot be modeled in an axisymmetric storm.

Since the storm motion is not represented in the axisymmetric storm, the storm motion vector was subtracted from observed winds at each level of the ingested sonde data. This removes the observed bias of stronger winds to the right of the center, and weaker winds to the left of the center. The speed of storm motion was calculated in a simple manner by determining the distance between the center fixes just before and just after the time of the wind observation and dividing that by the elapsed time.

One of the challenges of working with this data has been calculating the correct position of the center of the storm. The "best-track" datasets provided by the National Hurricane Center give locations in tenths of a degree of latitude and longitude. A combination of "best-track" and advisories was initially used to provide center fixes; however this proved to be of inadequate resolution. As will be shown later in this paper, the radial component of the wind is used in most of the budget calculations. Even small errors of less than 0.1 degree of latitude/longitude can cause large changes in the radial winds, especially for measurements close to the center, leading to unrealistically large inward or outward mass fluxes. Thus, even better fixes are required, as was noted in Riehl and Malkus (1961).

Along with the flight-level data, HRD provides high resolution storm tracks, based on a combination of radar, satellite, reconnaissance aircraft, and dropsonde data. For the cases considered here (Floyd, Georges, and Mitch), radar images are available at the time of some of the drops, allowing much more precision in fixing the center location. These help to make good first guesses of the center position, but another method for generating the track is needed.

4.1.3 Storm Track Calculation

To get the most accurate tracks, probabalistic track estimation was used to get the best storm track; this method also gives an indication of the dependence of the calculations on the track uncertainties. We can rate the acceptability of the newly-generated track, according to dynamical constraints, and use this scoring as a guide to the validity of the results produced by analyzing the storm against this track.

There are 4 steps in applying the track estimation method:

1. Generate the new track, by adding an offset to the first-guess track.

2. Calculate a cost function for this track; do this with the goal of choosing tracks with the smallest radial velocities at around 700mb.

3. Fit all of the observed sounding and flight-level data onto an axisymmetric grid defined by this track.

4. Calculate the momentum and energy budgets, and output the derived values for C_d and C_k, along with the track's score.

The most accurate track provided by HRD is the one included with the flight-level data [Edward Rahn, HRD, personal communication]; this is used to seed the routine. The track will be estimated over a period from 12 hours before the first sounding used, to 12 hours after the last sounding. This will permit an accurate evaluation of the storm motion for any times when we have sounding data. A sample track is shown below in Figure 4-1.

To model the path of the storm, several points are chosen from the inital guess path at equally spaced times over the period of interest. In the case of Floyd and other storms with

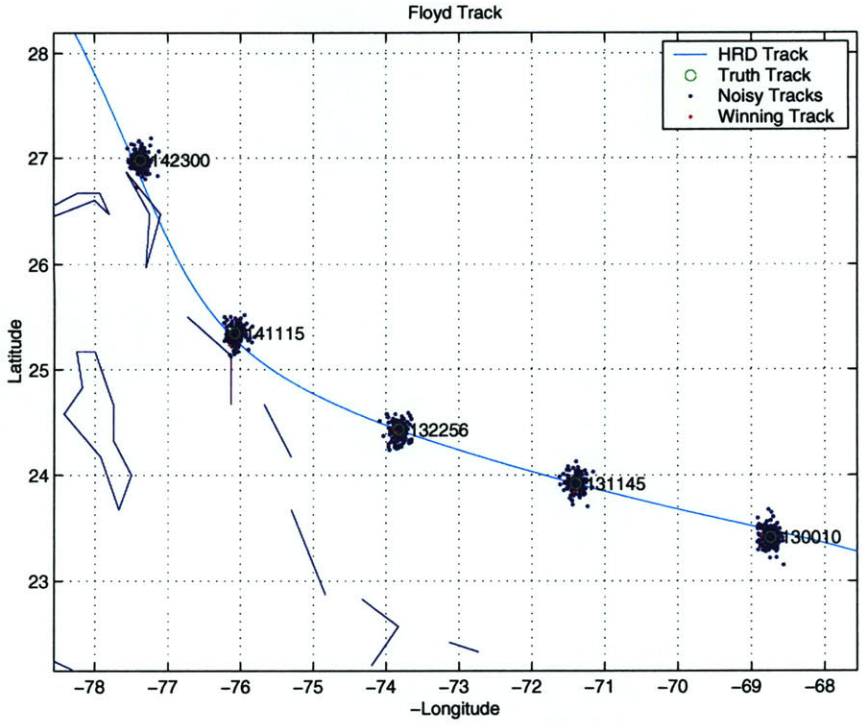

Figure 4-1: Floyd Track Estimates

slowly-varying paths, only a few points must be chosen. For storms with more complex paths, more points may be needed. The number of segments used for storms in this study was 5, unless otherwise noted. After a first guess track has been established, the new tracks must be generated. A Gaussian distributed error, with a standard deviation of $.1^o$, is added to the initial positions. Precisely, this is phrased as a displacement from the initial position of standard deviation $.1^o$, in a direction chosen randomly between 0 and 2π radians. The value of $.1^o$ was selected because the initial guess from HRD, especially at the times of reconnaissance flights, is based on the combination of radar, flight, and sounding data, and should be quite accurate. Their estimates, though, are for the center of circulation – this is not always at the center of the eye; it can be offset. For these budget equations, the exact eye dynamics are of no concern; rather, the center of the circular eyewall is needed to transform to a cylindrical coordinate system. Thus, the errors that are concerned with would consist mainly of the deviations of the circulation center from the center of the eye. Since the eye is quite small, especially in intense storms, with a radius on the order of 10-50km, the chosen standard deviation ought to cover most cases.

Once all of the points for the new track have been assigned, the storm motion vector is calculated for each segment. This is used to convert all of the earth-relative winds to storm-centered winds, which are used for the remaining calculations. Thus, the changes to the storm position feedback into the analysis of the winds by changing the location in potential radius space, by altering the amount of storm motion removed, and by modifying the angle used to transform from u and v winds to radial and tangential winds. The complicated nature of the transformations that must be made to both the wind components and the location in potential radius coordinates means that this problem is better suited to this probabalistic approach rather than attempting to calculate backwards from the final analyzed winds.

Ranking of Tracks

Once all of the positions in the track have had noise added, an evaluation of the validity of the track is performed. Observations and theory indicate that radial velocities in a hurricane generally show inflow near the surface, and an outflow layer in the upper troposphere. At mid-levels, radial motion is generally small. Thus, to rank the newly generated track, we assign it a score that is the sum of the square of all of the radial velocities of appropriate observations. For the flight-level data, all observations at the 650mb and 700mb pressure levels are used in the scoring. For the dropsondes, the observation from each sonde at 700mb is chosen. Since there are many data points for each flight (299), and only the single one for the sonde, a larger weight was assigned to the sonde value. This works to prevent the sonde contributions from being overwhelmed by the flight-level contributions. After the storm has been scored, the data is composited into the potential radius vs. height grid, and the flux calculations are performed.

The validity of this method for choosing storm tracks can be assessed by examining the wind and thermodynamic fields of the resulting composite. The vertical velocity, which is calculated by invoking conservation of mass, is quite sensitive to an accurate assessment of the storm center and motion. Even the tracks supplied by HRD with the flight level data, while far more precise than those based on 6-hourly advisories, yield vertical motion profiles that do not always look realistic. We can see in Figure 4-2 that the vertical motion

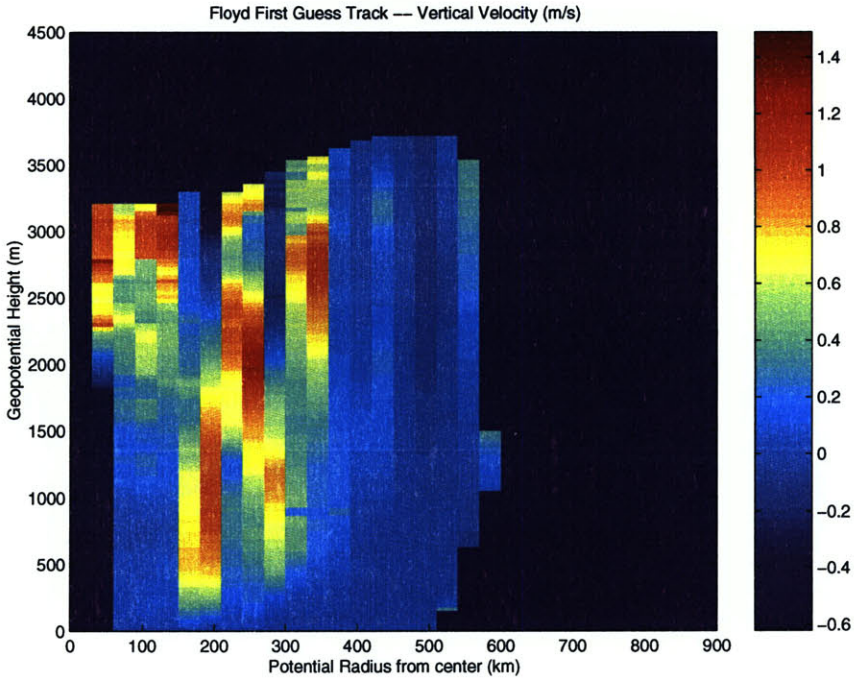

Figure 4-2: w for Floyd, HRD track

is upward in the area of the eyewall, but that motion is quite patchy, and not really what we might expect from the vigorous convection of the eyewall (which should be almost entirely free of downdrafts). The vertical velocities shown in Figure 4-3, however, show two distinct regions of upward velocity. Radar images of Floyd (Figure 3-1) from the same times show two concentric rings of convection, which matches very well with the profile shown here. The reasonable distributions of vertical motion, which is sensitive to small changes of track information, helps us to conclude that the scoring method is sound.

4.1.4 Best Estimates and Variance of Coefficients

Once all of the estimated paths have been generated and the coefficients computed based on each one, we have an ensemble of tracks whose coefficients can be interpreted. We can define a cost function which provides a measure of how close to truth we think each track is. For this work, the parameter which serves to rank the paths is the radial velocity at mid-levels (650-700mb). In a steady hurricane, this will generally be close to zero; with inflow at low levels of the storm and outflow at high levels, near the tropopause. Thus, a

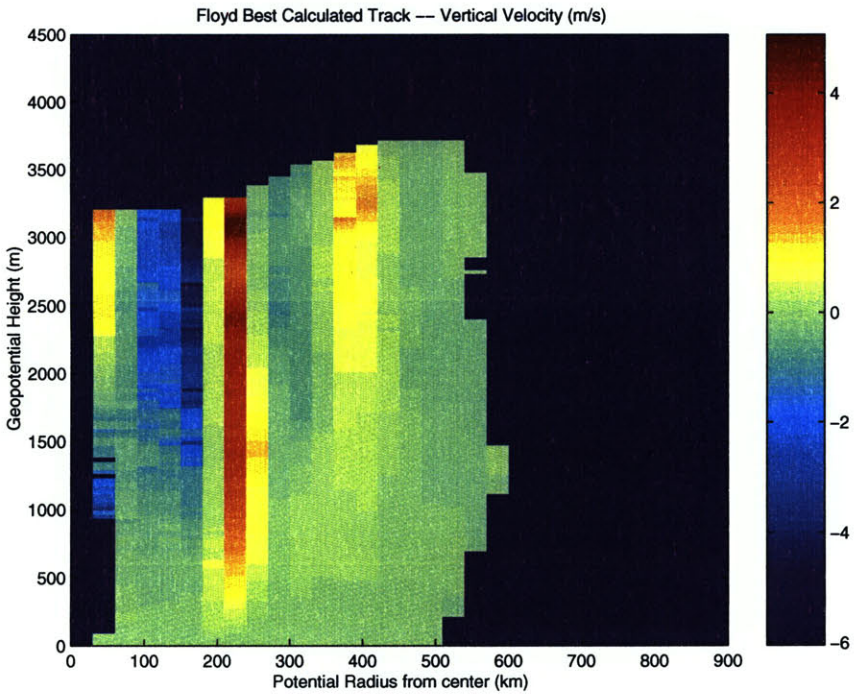

Figure 4-3: w for Floyd, best calculated track

track will receive the best ranking if all of the computed radial velocities are close to zero. Then, a distribution of the transfer coefficient values can be analyzed, using a weighting based on how probable their corresponding tracks are.

The definition of the cost function for rating tracks is:

$$C(f_a) = \sum_{k=1}^{K} w_k \left[f_a(x_k) - f_o(x_k)\right]^2 \tag{4.4}$$

where C is the cost function, for a set of observations $f_o(x_k)$ where $1 \leq k \leq K$, where K is the number of observations. For our purposes, f_o is the radial velocity of the observation. Then f_a is the expected value; here that is 0. The weighting is w_k; with the only choices based on the type of observation. Flight data has a weight of 1, sounding data has a weight of 10. The flight data is given a smaller weight because each flight has many observations which are at the level of interest; in addition these generally are somewhat correlated with one another. The dropsondes, on the other hand, only provide one observation at the 700mb level. This weighting allows the signal from the dropsonde observations to remain in the

cost function, rather than being overwhelmed by the sheer number of flight observations. The best track is chosen as the one with the lowest value of C; that is, the composite which has the smallest total value of radial velocity squared at flight level.

The same methodology that was used to rate the probabalistic tracks will also produce uncertainty information for the values of the transfer coefficients. The values can be weighted using the cost function values from the track estimates, using Equation 4.5. Then they can be averaged, taking into account the desirability of each track, and deviation statistics also produced. From this, a better understanding of how the changes in the track of the storm affect the coefficient values can be obtained.

$$W = \frac{C_{max} - C}{C_{max} - C_{min}} \tag{4.5}$$

Here, W is the weight, a number between 0 and 1; C_{max} is the largest value of the cost function in the entire ensemble, C_{min} is its smallest value for the ensemble, and C is the cost function for the individual track.

We can then calculate a weighted mean, M, and deviation, D, where C_{dn} is the drag coefficient calculated for track n:

$$M = \frac{\sum_{n=1}^{N} W_n C_{d_n}}{\sum_{n=1}^{N} W_n} \tag{4.6}$$

$$D^2 = \frac{\sum_{n=1}^{N} W_n^2 (C_{d_n} - M)^2}{\sum_{n=1}^{N} W_n^2} \tag{4.7}$$

The same method is used to calculate the mean and standard deviations for C_k.

4.1.5 Compositing the Data

Choice of domain and resolution

In order to calculate the values for the exchange coefficients, we need to examine the budgets of heat and angular momentum at various radii in the storms. The transformed potential radius has a magnified scale in the eyewall, so that instead of being perhaps 30-60km from the center in physical space, the eyewall in potential radius space lies between about 200km and 400km for the storms analyzed in this study. Since the heat and momentum transfer are

expected to be strongest in the regions with high wind speeds, including the eyewall, this entire region must be included in our domain. Based on the distribution of observations, an outer edge of 900km in potential radius coordinates was chosen; this allows a clear view of where the eyewall ends on the outer edge. The calculations of C_k and C_d were performed over the entire radial domain, but the averages presented here are only for the eyewall region, as identified by moisture and wind profiles for each storm.

The most convenient way of calculating the angular momentum and heat budgets would be to integrate from the surface through the depth of the troposphere, but most of the sondes were dropped from a flight level at about 650mb. In the absence of upper-level data to quantify the outflow from the hurricane, analysis of just the inflow layer can instead be accomplished. Instead of using a rigid top to the atmosphere, we can calculate the vertical fluxes out of the inflow layer based on w. This region is assumed to have relatively small values of eddy fluxes (Hawkins and Rubsam, 1968), so this approach should accurately produce budget results. It is crucial to note that this approximation is only valid in the eyewall, where the fluxes are due to the larger scale upward vertical motion, which can be explicitly resolved (Emanuel, 1986). The eye is not characterized by a balance between surface fluxes of enthalpy and momentum, but rather is governed by turbulent entrainment from the eyewall and subsidence from near the tropopause. Outside of the eyewall, turbulent vertical fluxes dominate the enthalpy and momentum budget; this means that most of the transfer would not be accounted for by the time and azimuthally averaged vertical motions, but by small time and space scale features, such as downdrafts. Thus, only in the eyewall should we expect the budget equations to be valid.

Height coordinates were chosen for the vertical axis for ease of specifying the lower boundary. In pressure coordinates, the surface slopes upwards toward the center of the storm; all cases analyzed here are for hurricanes at sea, so the the lower boundary in height coordinates is just 0m. This simplifies calculations by producing boxes of equal size and orientation. Due to the availability of data, an upper bound of 4500m was chosen, which should capture all inflow. This height also allows the flight-level data to be included in the composite.

Sensitivity of the Compositing

While in most ways the availability of high resolution is a positive factor, it introduces some complexities that must be dealt with. In particular, observations which appear to be regular in physical space can end up transformed in potential radius coordinates to areas of very sparse and very dense data. The details of the radial transformation depend on the tangential wind field; a storm with winds that change gradually with physical radius will have a uniform mapping into potential radius space; a storm with a sharp tangential wind maximum will present a profile of rapidly increasing potential radius with physical radius inside the radius of maximum winds(RMW), then potential radius will remain nearly constant as radius increases (but wind decreases) outside of the RMW. For the storm to remain inertially stable, the potential radius and physical radius must always increase together, though at different rates. Some storms, though, may approach this limit quite closely, as we will later see.

Since the sondes measure only the immediate environment through which they fall, they will detect a number of small-scale features, such as convective updrafts, wind gusts, and local bursts of convection. In addition, while we idealize the storms to be axisymmetric, there will be both small-scale and large-scale deviations from this, all of which may be detected by the dropsondes. Instrument bias and error and deviations in the horizontal and vertical positioning of the sonde will also add error to the data set. These measurement errors are thought to be rather small given the recent improvements in the sonde technology (Hock and Franklin, 1999), and at least are an improvement over previous models. While working with the data, for most cases where values departed from consistency checks (such as pressure increasing with distance from the center, or equivalent potential temperature increasing toward the center) asymmetry of the storm appeared to be the most logical explanation. In adjusting the center fixes, these factors were taken into account to yield results where pressure, thermodynamic quantities, and wind fields all appeared reasonable.

Smoothing and Averaging

The other difficulty with the high resolution data is that at times strong radial gradients of various fields were introduced. These small-scale gradients led to large values of some of

the derived quantites. For example, high-frequency variations of radial wind lead to very strong, narrow bands of upward and downward vertical motion, since w is calculated from the continuity equation. In order to smooth the data to give a larger-scale view of variations, the data was divided into bins with horizontal (radial) resolution of 60km in potential radius space and vertical resolution of 30m. When several observations mapped into one box, the observed values were averaged. Especially for the wind observations, this seemed to smooth the very high resolution changes likely associated with wind gusts to provide a detailed, but slowly varying wind profile. The radial resolution approximately matches the distribution of sonde drops – around 25 sondes were generally dropped in the inner 120km of the storm. In the vertical, boxes of 30m were used, giving very high resolution while allowing some averaging of data in each box. Since the sondes generate readings at about 5m intervals as they fall, this gives 5-6 readings per box for each sounding. This resolution is a compromise between the sparse data regions of the inner eyewall and the data-rich areas of the outer eyewall (past RMW), such that a reasonable number of observations are ingested into each radial band.

Interpolation

Once the averaged quantities are calculated, interpolation is used to fill in areas where no data are present. Interpolation was done only in the horizontal, with interpolated values based on the data at the same height at the nearest points in the positive and negative radial direction. The chosen vertical compositing resolution always yielded data in each box where a sonde fell, so before interpolation the data gaps were vertical columns. Average values are calculated for density, total energy, enthalpy, surface pressure, radial wind, tangential wind, and angular momentum. Radial wind is calculated by interpolating the value of the radial mass flux at the inner and outer readings. Note that angular momentum is averaged, not recalculated from interpolated winds because the original calculations of angular momentum include f, which is not represented in the radial composite.

Calculation of derived quantities

Radial Wind The radial component of the wind is calculated for each level of the sounding, after removing the motion of the storm itself from the observed wind. This is calculated by determining the location of the center of the storm at the time of the observation, and then splitting the wind into the radial and tangential components. The sondes move appreciably around the center of the storm in the time that elapses between launch from the aircraft and splashdown in the ocean, sometimes rotating more than 45 degrees around the center if dropped into the eyewall. Thus it is important to use the location data at each level and not think of the sonde as a vertical set of observations; rather it is a helical pattern. Once the location of the observations have been mapped into the radial coordinates, it generally shows descent at a constant radius at higher levels, with increasing motion towards the center as it approaches the ground, indicative of low-level inflow.

Tangential Wind Tangential wind is derived in a similar way to the radial wind.

Vertical Motion Vertical motion is derived by enforcing a mass balance for each "box" in the grid. Each box actually represents an annulus at a given distance from the center and of the incremental height. For each annulus that is in contact with the surface, the vertical mass flux out of its top is simply the difference between the incoming and outgoing horizontal mass fluxes. No vertical mass flux is possible at the surface (we are here neglecting the moisture flux from the surface which has only a minor effect on the mass field). Above this level, mass fluxes across the outer and inner boundary are calculated, then the vertical motion out of the top of the box is calculated, taking into account the vertical influx from below. This method is generally inappropriate for synoptic scale flows and observations, since vertical motions there are quite small (a few cms^{-1}), and soundings are widely spaced (several hundred km apart). In hurricanes we have the benefit of rather strong expected upward motion of between 1 ms^{-1} to perhaps 10 ms^{-1} in individual convective elements. By performing the radial compositing of data, we also have very high horizontal resolution, averaging better than a sounding every 10km. These two features make calculating mass convergence a practical way of deriving vertical motion.

Interestingly, vertical motion is available directly in the sonde data, but it is highly variable, sometimes changing more than 2 ms^{-1} over a vertical distance of 100m. This variability indicates that the sonde is measuring scales of motion that we would classify for this study as turbulent eddies. In addition, this motion is calculated from the difference between the actual rate of descent and the theoretical rate under calm conditions (Hock and Franklin, 1999). Given the strong horizontal winds, wind shear, and the presence of precipitation that one would expect to find under hurricane conditions, imputing all deviations from a theoretical fall speed to the actual vertical velocity of the air seems optimistic. Thus, these observations were not used in the calculations, in favor of the derived values. The derived vertical motion results vary quite slowly in the vertical, due to the nature of the calculation, but quite clearly capture expected features of the circulation, such as descent in the eye and strong upward motion in the eyewall, as can be seen in Figure 4-3. The vertical motion is not used explicitly in any of the budget equations, but is calculated for diagnostic use to verify that the analyzed wind fields are reasonable.

Angular Momentum Angular momentum, Equation 1.1, is calculated for each data point in the soundings, then aggregated into the radius/height boxes.

Total Energy Total energy, Equation 1.4, is used to perform the budget of heat transfer, in order to calculate C_k. Total energy is just enthalpy plus potential energy and a term to include the kinetic energy of the wind itself. The kinetic energy term is usually not considered, since for synoptic-scale disturbances it is generally small compared to the other terms. In a hurricane, with high wind speeds, it is a more important factor.

Frictional dissipation of wind speed can be thought of as transferring energy from the kinetic energy of the wind to the kinetic energy of the gas itself by raising its temperature. By including the wind in the total energy equation, the process is captured so that wind energy that is converted into heat remains accounted for in the system. For a hurricane this energy transformation will occur most strongly at the surface in the inner radii of the hurricane, where this extra heating of the air goes directly into fueling the convection in the eyewall, and thus maintaining the strength of the storm.

It can be seen that total energy, E, is just enthalpy, k, (Equation 1.3) plus the gravita-

tional and windspeed components. Enthalpy can then be considered to be a special case of total energy for calm conditions at the surface. Thus, the energy budget we use for total energy will consider fluxes of total energy through the radial edges and the upper edge, and the flux of enthalpy across the lower boundary.

4.1.6 Smoothing

A modified version of a three-point smoother was applied to the θ_e and physical radius fields. For θ_e, a nine-point smoother was used – all of the adjacent grid boxes in the horizontal (60km in width, potential radius space) and vertical (30m in height) were used to smooth the value of the center box. This worked to smooth what were sometimes irregular small-scale horizontal variations. For physical radius, where most of the small-scale variation was noted in the vertical (probably due to gusts in the tangential wind), smoothing included the grid boxes one grid-spacing inward and outward radially, and 10 levels upward and downward, with diminishing weighting with distance.

Chapter 5

Angular Momentum Calculations

5.1 Budget of Angular Momentum

The budget of angular momentum will be calculated by considering an axisymmetric storm that does not vary in time. The cases analyzed have been chosen to match these constraints within reasonable limits. The momentum equation in cylindrical coordinates yields the following expression, shown in equation 5.1, for the shear stress in the azimuthal direction, τ_θ, due to surface friction, where evolution in time has been neglected. As this is phrased in cyclindrical coordinates, u is the radial velocity, and w is the vertical velocity.

$$\nabla \cdot (\rho \mathbf{u} M) = \frac{1}{r}\frac{\partial}{\partial r}(r\rho u M) + \frac{\partial}{\partial z}(\rho w M) = r\frac{\partial \tau_\theta}{\partial z} \tag{5.1}$$

Multiplying equation 5.1 by r leads to equation 5.2.

$$r\nabla \cdot (\rho \mathbf{u} M) = \frac{\partial}{\partial r}(r\rho u M) + \frac{\partial}{\partial z}(r\rho w M) = r^2\frac{\partial \tau_\theta}{\partial z} \tag{5.2}$$

Now we integrate over the annulus radially from r_i to r_o, and vertically from the sea surface to the top of the PBL, z_b.

$$\int_{r_i}^{r_o}\int_0^{z_b} r\nabla \cdot (\rho \mathbf{u} M) dz dr = \int_{r_i}^{r_o}\int_0^{z_b} r^2\frac{\partial \tau_\theta}{\partial z} dz dr \tag{5.3}$$

Since we have assumed that the storm is axisymmetric, we do not need to consider

any azimuthal variations. In addition, since the surface stress is only present at the lower boundary, the only contribution to the vertical integral is at $z = 0$, where $\tau_\theta = \tau_{\theta 0}$. Since the integrals will be evaluated over narrow radial boxes, we can also assume that $\tau_{\theta 0}$ does not vary with radius. We thus achieve:

$$r_o \int_0^{z_b} \rho u M dz - r_i \int_0^{z_b} \rho u M dz + \int_{r_i}^{r_o} r \rho w M dr = -\frac{1}{3}(r_o^3 - r_i^3)\tau_{\theta 0} \tag{5.4}$$

For the next steps in the derivation, we would like to incorporate mass continuity into the equations so that the vertical motion does not explicitly appear. The mass continuity equation in cylindrical coordinates is shown in equation 5.5.

$$\frac{\partial}{\partial r}(r\rho u) + \frac{\partial}{\partial z}(r\rho w) = 0 \tag{5.5}$$

Integrating equation 5.5 over the depth of the boundary layer and from r_i to r_o produces equation 5.6, which can be seen to be similar in form to equation 5.4:

$$r_o \int_0^{z_b} (\rho u) dz - r_i \int_0^{z_b} (\rho u) dz + \int_{r_i}^{r_o} (r \rho w) dr = 0 \tag{5.6}$$

We now choose a value of angular momentum M_t so as to satisfy:

$$\int_{r_i}^{r_o} r \rho w M dr = M_t \int_{r_i}^{r_o} r \rho w dr \tag{5.7}$$

We now multiply equation 5.6 by the average value of angular momentum over the top edge of the annulus, M_t, and subtract it from equation 5.4, as shown in equation 5.8. This has the effect of removing the explicit vertical motion, since M_t times the third term of equation 5.6 is identically equal to the third term on the left-hand side of equation 5.4. Instead, the vertical flux is implicit in the difference between the two radial flux terms. The surface stress, on the right-hand side of the equation, has been expanded using the bulk aerodynamic formula. Here, v_{10} is the tangential wind at 10m, and $|\mathbf{V_{10}}|$ is the magnitude of the 10m wind.

$$r_o \int_0^{z_b} \rho u(M - M_t)dz - r_i \int_0^{z_b} \rho u(M - M_t)dz = -\frac{1}{3}(r_o^3 - r_i^3)\rho C_d v_{10}|\mathbf{V_{10}}| \quad (5.8)$$

This equation can then be evaluated for each column in the grid to yield a value for C_d. We find it convenient to use a grid box framework based on potential radius coordinates, and since the limits of integration are within the boundary layer, the modified version of potential radius is used (see equation 4.2). Angular momentum, however, is calculated with the actual wind speeds in the boundary layer. In the boundary layer, this modified coordinate has a constant mapping between potential radius and physical radius, which does not vary with height. Equation 5.8 is thus evaluated using the physical radius of the grid boxes for r_o and r_i. The benefit of the potential radius coordinate is that higher resolution is available in the eyewall of the storm, but otherwise the equations are phrased simply in physical coordinates.

As an aid to modeling work, where 10m winds are often not calculated, the drag coefficient can also be calculated based on values of wind and density at the top of the boundary layer, where gradient balance holds. This allows the behavior of the boundary layer to be parameterized just using C_d. The formula for computing C_{dGrad}, the gradient level drag coefficient, is given in equation 5.9.

$$r_o \int_0^{z_b} \rho u(M - M_t)dz - r_i \int_0^{z_b} \rho u(M - M_t)dz = -\frac{1}{3}(r_o^3 - r_i^3)\rho_{grad} C_{dGrad} v_{grad}|\mathbf{V_{grad}}| \quad (5.9)$$

It should be noted that this line of reasoning neglects the turbulent flux of angular momentum; under the conditions of the hurricane eyewall this is a justifiable simplification. The turbulent fluxes of angular momentum at the top of the boundary layer are small due to the small vertical gradient of angular momentum there. Radial turbulent fluxes of angular momentum are thought to be small for all regions of the hurricane, with the notable exception of the inner edge of the eyewall. Radial turbulent fluxes are an important source of angular momentum to spin up the eye (Emanuel, 1995a), so the above equations are not to be considered valid there.

Chapter 6

Momentum Budget Results

6.1 Overview

Observations from three hurricanes were analyzed. Of the three (Floyd, Georges, and Mitch), Hurricane Floyd proved to be the most amenable to the compositing process, which was described in section 4.1.2. How the other storms deviated from idealized profiles will be discussed in this section. Due to the simple format of the budget for C_d (see equation 5.8), reasonable values were obtained for all three storms from the budget. The calculation of C_d has turned out to be quite robust – it has a consistent value over the 3 storms. This is in part due to the form the advective equation takes in potential radius coordinates; vertical motion is incorporated implicitly into the equation.

6.2 Hurricane Floyd Results

6.2.1 Floyd Track Selection

At the time of the of our analysis, Floyd was passing just to the east of the Bahamas, and beginning to recurve northward. The track was slowly varying, so a track estimate of 5 initial points over two days was selected for the track estimation scheme. Two hundred iterations were run, with an offset of standard deviation $.1^o$ at each of the 5 points. This seems to be a reasonable estimate of the potential error in the center fixes for the hurricane. Most likely, the main cause of deviation from the HRD best track is that they fix the center

Quantity	Mean Value	Standard Deviation
10m C_d	0.0027	0.0018
Top 10% 10m C_d	0.0033	0.0018
Gradient C_d	0.0022	0.0018
Top 10% Gradient C_d	0.0026	0.0016

Table 6.1: Momentum Transfer Coefficient Values for Floyd

as the location of the pressure minimum within the eye; for the purposes of calculating radial winds, a more useful fix is the geometrical center of the eyewall. Small-scale dynamics can cause the pressure center to wobble within the eye, without having a significant effect on the overall circulation in the eyewall. The final track chosen is shown in Figure 4-1. We note that the highest scoring values selected are at most about 1 standard deviation away from the intial track positions.

6.2.2 Floyd Momentum Budget

The drag coefficient values for the optimal track, averaged over the grid boxes in the eyewall are shown in Table 6.1. The mean 10m wind speed over this region (210km to 450km, in R-space) was 43.17 m/s, with a maximum single gridbox value of 51.93 m/s.

The values of C_d that were produced by all of the ensemble members were averaged, weighted by the score given to each track, to give more influence to values for tracks which are ranked better. In addition, values of C_d less than zero, which is not a physically meaningful result, have been excluded, as have those with values greater that 0.01.

This analysis produces a mean value for C_d of 0.0027 with a standard deviation of 0.0018. If only the top 10% scoring values are used, we get a mean value for C_d of 0.0033 and a standard deviation of 0.0018.

The values for the momentum coefficient are well within the range of values reported in the literature, which generally range from .001 to .004 for high windspeeds (see section 2). The uncertainty associated with this value can be determined by using the distribution of values for all of the 200 track variations. The distribution of 10m drag coefficient values for the ensemble members is shows in Figure 6-1. The mean value is indicated with a solid line, and the standard deviation is shown by the dashed lines.

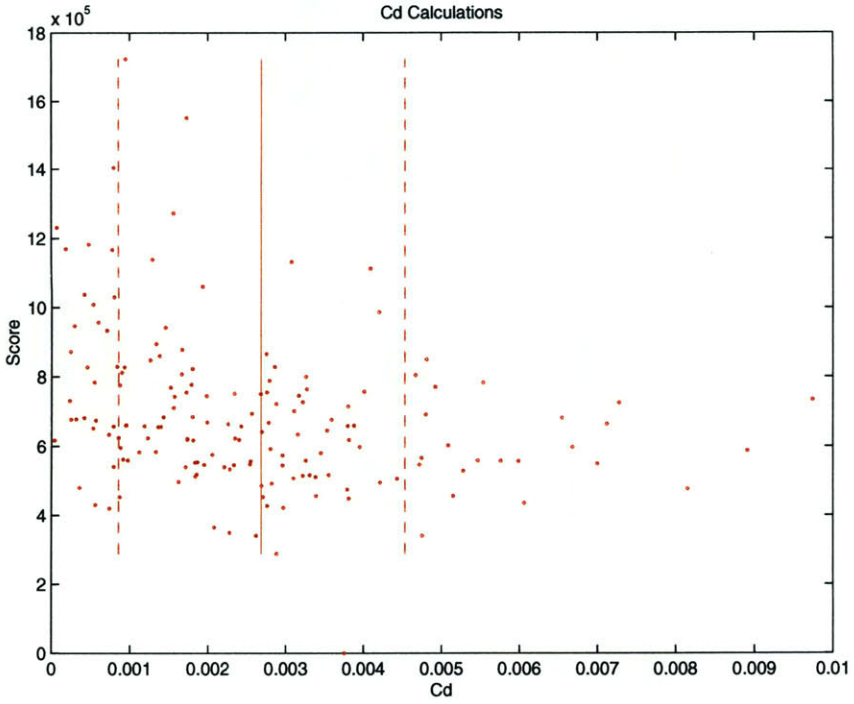

Figure 6-1: Floyd Coefficient Estimates

6.3 Hurricane Georges Results

At the time of the dropsonde measurements, Georges was moving along a smooth path in the open Atlantic east of the Lesser Antilles. Since the track was slowly varying, a track estimate of five initial points over two days was selected for the track estimation scheme. Two hundred iterations were run, with an offset of standard deviation $.1^o$ at each of the five points.

The distribution of drag values for Georges is shown in Figure 6-3, and in Table 6.2. For Georges, four outliers were excluded from the averaging calculations: one was less than 0, and three were larger than 0.01. Of all of the storms analyzed, Georges produced the most tightly distributed range of values for C_d. Considering a distribution with the outliers removed is appropriate here because very few physical constraints were placed on the choice of track candidates; outliers are likely the result of compositing that produces badly distributed wind and thermodynamic fields.

The mean surface wind speed in the eyewall was 43.96 m/s, but there were soundings

Quantity	Mean Value	Standard Deviation
10m C_d	0.0028	0.00088
Top 10% 10m C_d	0.0029	0.00065
Gradient C_d	0.0012	0.00039
Top 10% Gradient C_d	0.0012	0.00024

Table 6.2: Momentum Transfer Coefficient Values for Georges

that recorded winds of more than 80 m/s. The standard deviation of the winds in the eyewall was 20 m/s. Winds in Georges changed very rapidly with physical radius, then decreased again rapidly outside the radius of maximum winds, as shown in Figure 6-2. When transformed into potential radius coordinates, this causes a large increase in resolution where winds are increasing with radius, so that a position at 15km in physical radius coordinates can be mapped as far as 250km out in potential radius coordinates. When observations are composited into this regime, large gaps occur in potential radius space, requiring interpolation. Then in the region of decreasing winds with radius, physical space is squashed. A more tricky problem is that observations in the decreasing wind region all fall quite close together, and any small variations due to error or storm asymmetry can cause a composite that is inconsistent with the basic physics governing it. A regular pattern of observations in physical space would transform into sparse measurement of the area just inside the radius of maximum wind, and very dense observations outside of it.

For a circulation to remain intertially stable, it must have a monotonically increasing physical radius with potential radius. However, a storm can approach this limit quite closely, as it appears to be doing in the case of Georges, which had just finished explosively intensifying at the time of the observations.

For Georges, the calculations yield a mean value for C_d of 0.0028 and a standard deviation of 0.0009. If only the top 10% scoring values are used, we get a mean value for C_d of 0.0029 and a standard deviation of 0.0006.

6.4 Hurricane Mitch Results

Mitch was a problematic storm for the track estimation routines, because its path over the time of interest was very erratic. In order to choose the best track, 20 interpolation points

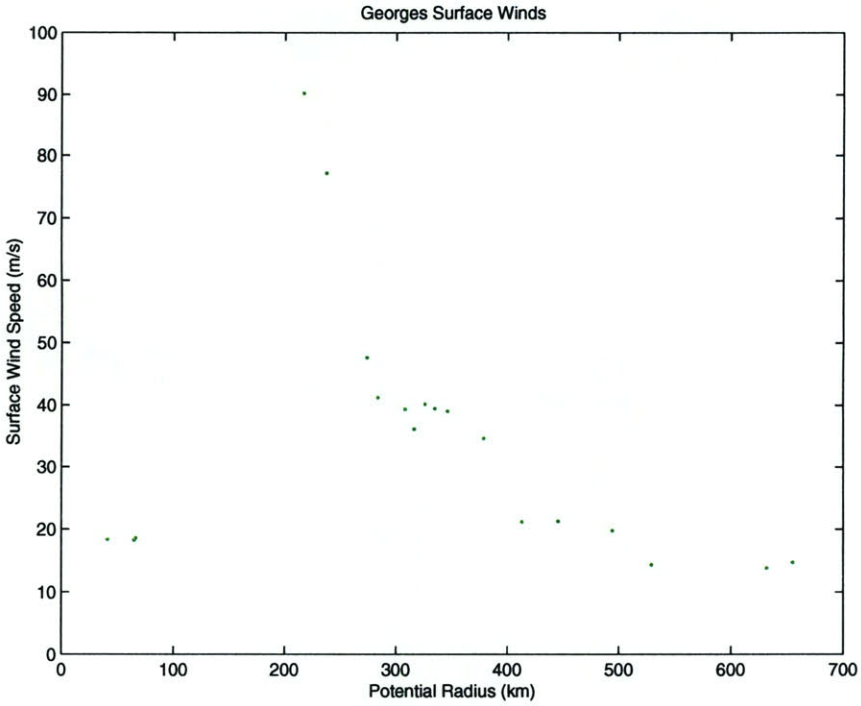

Figure 6-2: Georges Surface Winds

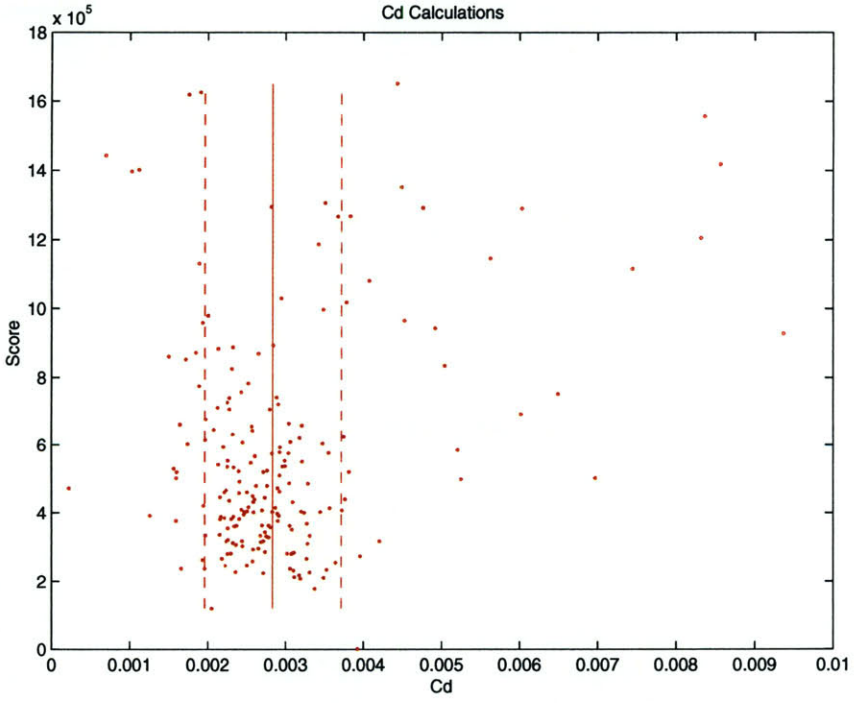

Figure 6-3: Georges Coefficient Estimates

Quantity	Mean Value	Standard Deviation
10m C_d	0.0043	0.0015
Top 10% 10m C_d	0.0048	0.0011
Gradient C_d	0.0022	0.00091
Top 10% Gradient C_d	0.0023	0.00070

Table 6.3: Momentum Transfer Coefficient Values for Mitch

were used, and 1800 noised tracks were tested. This is shown in Figure 6-4; the resultant best track is shown in Figure 6-5. Note that the "truth" track is the first guess track based on the HRD track files. The "Winning" track is the one selected as best by the estimation routine.

Another difficulty in evaluating Mitch is that many sondes did not quite reach the surface, but failed in the last few hundred meters above the sea surface. These failed sondes recorded much higher winds (just before failure) than the rest of the sondes that provided observations all the way to the surface; this suggests that the high winds might be the cause of the failure. These sondes recorded winds of 70-90 m/s not far above the surface. However, this selective failure of sondes in the areas of strongest winds reduced the averages of 10m winds artificially. The average 10m wind over the eyewall region (240km-420km in potential radius coordinates) was 39.9 m/s, with a maximum grid box value of 53.14 m/s. Based on the values from the failed sondes, and the wind profiles of the successful sondes, it seems likely that 10m winds in excess of 60 m/s were occurring in the eyewall. As an example of how this would change the value of C_d, a stress which yields C_d=0.0040 for a surface wind speed of 50 m/s would produce a C_d value of 0.0028 for a surface wind speed of 60 m/s. Both other cases had few sonde failures in the lowest levels, so that 10m winds were more likely to be better representations of the actual conditions. Note that the gradient level calculations for the drag coefficient should be only minimally sensitive to this problem, as the loss of data in calculating the stress through the depth of the boundary layer will be a relatively small effect.

The drag coefficient values are shown in Figure 6-6 and Table 6.3. For Mitch, the mean value for C_d of 0.0043 with a standard deviation of 0.0015. If only the top 10% scoring values are used, we get a mean value for C_d of 0.0048 and a standard deviation of 0.0011.

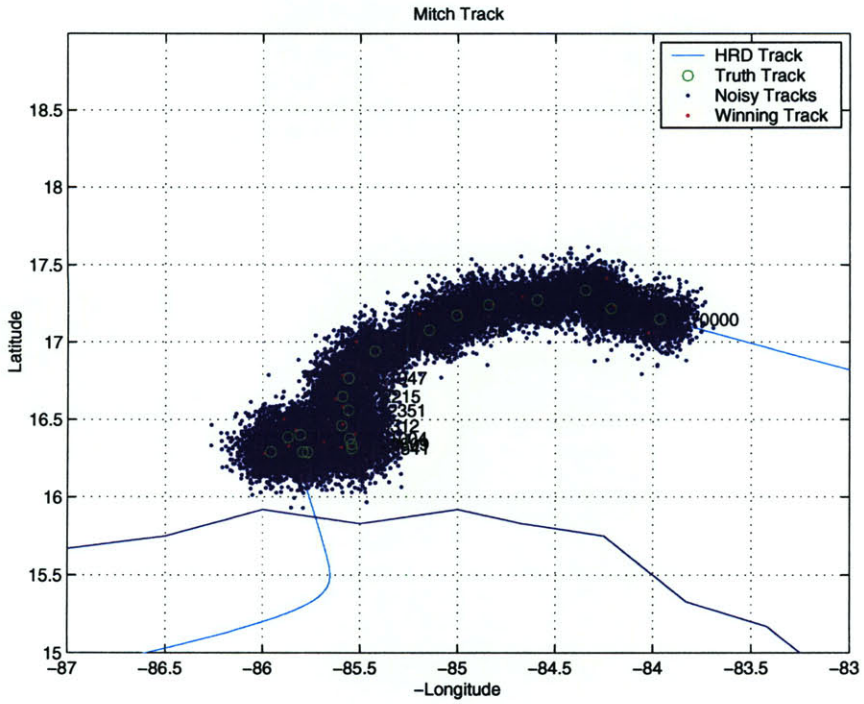

Figure 6-4: Mitch Track Ensemble, with best track

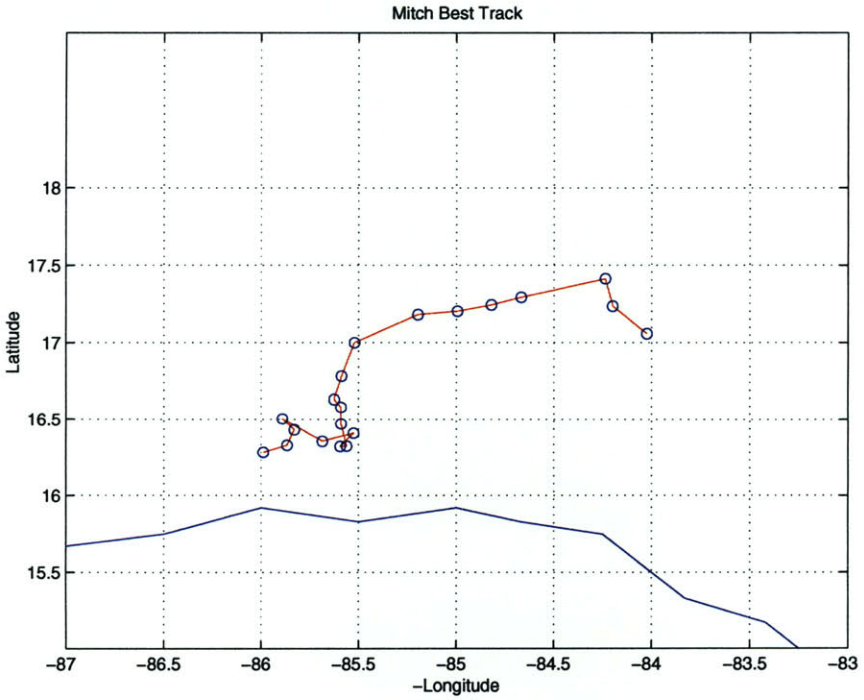

Figure 6-5: Mitch Best Track chosen from Ensemble

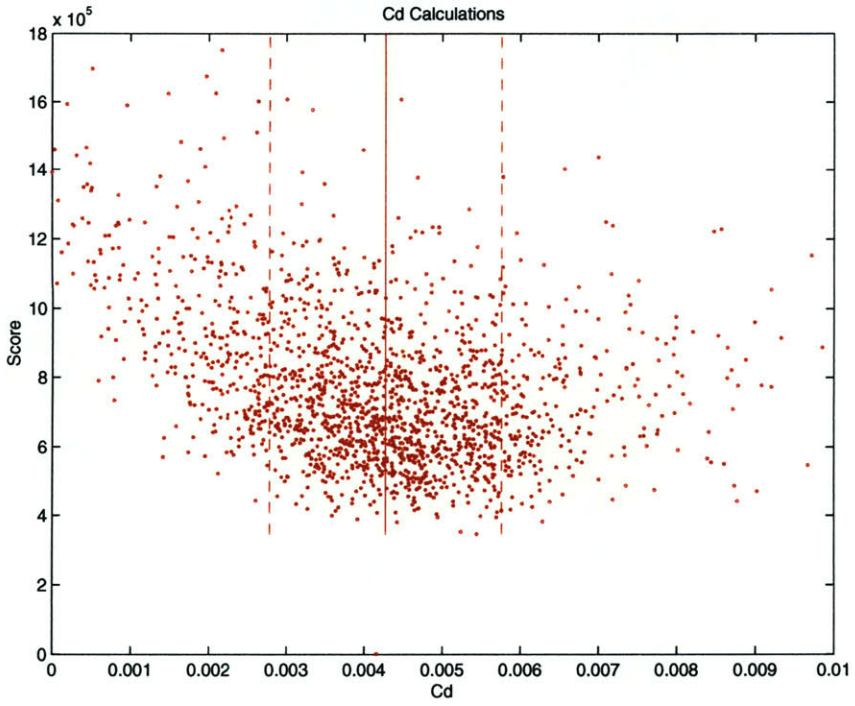

Figure 6-6: Mitch Coefficient Estimates

6.5 Summary

We note that all three hurricanes had similar wind speeds, so the values for C_d can be compared. These are summarized in Table 6.4. The 10m values show an average of 0.0033 and a mean standard deviation of 0.0014. The gradient level values have a mean C_d of 0.0019 and a mean standard deviation of 0.0010. It is interesting to note that the 10m and gradient level calculations for each storm do not show much consistency. That is, while Floyd and Georges have similar 10m values of C_d, the gradient level C_d values differ by nearly a factor of two. Meanwhile, the gradient level values for Mitch and Floyd are equivalent, but the 10m value for Mitch is significantly larger. This difference supports the idea that the surface winds for Mitch have a low bias due to the failure of dropsondes in the strongest winds in the eyewall, as noted above. An adjusted value of 0.0028 for 10m C_d based on a stronger surface windspeed is in line with the values for Floyd and Georges. This bias would affect the gradient level drag coefficient only minimally.

Quantity	Mean Value	Standard Deviation
Floyd 10m C_d	0.0027	0.0018
Floyd Gradient C_d	0.0022	0.0018
Georges 10m C_d	0.0028	0.00088
Georges Gradient C_d	0.0012	0.00039
Mitch 10m C_d	0.0043	0.0015
Mitch Gradient C_d	0.0022	0.00091

Table 6.4: Momentum Transfer Coefficient Values for all 3 Hurricanes

Chapter 7

Energy Budget

7.1 Energy Conservation Equation

The conservation of energy can be expressed as:

$$\frac{\partial}{\partial t}\left[\rho\left(U+\frac{V^2}{2}+gz\right)\right]+\nabla\cdot(\rho(k+\frac{V^2}{2}+gz)\mathbf{V}=-\nabla\cdot\mathbf{F} \tag{7.1}$$

Here, U is internal energy, defined as $U=(1-q_t)c_{vd}(T-T_0)+q_tc_lT+(L_v-R_vT)q$, V is the tangential wind, $\mathbf{V}$ is the full wind, k is the enthalpy, and $-\nabla\cdot\mathbf{F}$ is the energy flux.

Since we assume that the circulation under study is steady with time, we can simplify 7.1 to get:

$$\nabla\cdot(\rho(k+\frac{V^2}{2}+gz)\mathbf{V})=-\nabla\cdot\mathbf{F} \tag{7.2}$$

And we note that by our earlier definition, (equation 1.4), $k+\frac{V^2}{2}+gz=E$. Thus we have an equation for the conservation of total energy.

Discussion of the Energy Equation

$$E=(c_{pd}(1-q_t)+c_lq_t)(T-T_0)+L_vq+gz+\frac{V^2}{2} \tag{7.3}$$

The total energy has terms to represent the effects of enthalpy as well as the potential and kinetic energies. Thus a parcel ought to maintain its value of total energy during its

inflow into the storm and ascent into the eyewall, were it not for fluxes from the sea surface. Any change in the value of total energy of a parcel can then be attributed to heat exchange with the ocean. The addition of the $\frac{V^2}{2}$ term allows this quantity to subsume the conversion from kinetic energy of the wind to heating of the air caused by frictional dissipation of the wind. Any changes to the total energy then can be seen to have been caused by the addition of sensible or latent heat from the sea surface. As we are considering only the inflow and ascent through the lowest 3 km of the troposphere, and timescales of this motion will be rather small due to the strength of the inflow and updrafts, radiative effects will be assumed to be negligible and will be ignored. In a budget that also considers the upper levels of the hurricane, where slow outflow and subsidence are occurring, radiative cooling should be included.

The budget of total energy is calculated by considering the difference of the flux of total energy into the volume from flux of total energy out of the volume. This budget must be evaluated with the lower boundary at the sea surface and an upper boundary at either the top of the troposphere or the top of the inflow layer. Since the dropsonde data is only available over the lower troposphere, calculations in this work were performed for the inflow layer. At the top of the inflow layer, horizonal fluxes should be near zero, with all of the flux occurring vertically. When the lower boundary at the sea surface is chosen, any residual then must be the contribution from the air-sea flux.

7.2 Energy/Entropy Budgets

The budget equations for energy and entropy follow in a similar vein to those for angular momentum. The derivation presented here will remain general until the end, as there are several parallel energy variables (enthalpy, total energy, and entropy) that can be used. As before, the circulation will be idealized as steady in time and axisymmetric. Thus, for a conserved scalar field ϕ with a source term S:

$$\nabla \cdot (\mathbf{u}\rho\phi) = \mathbf{u}\rho \cdot \nabla\phi + \phi\nabla \cdot (\rho\mathbf{u}) = -S(\phi) \tag{7.4}$$

We can use the mass continuity equation ($\nabla \cdot (\rho\mathbf{u}) = 0$)to reduce this to:

$$\nabla \cdot (\mathbf{u}\rho\phi) = \mathbf{u}\rho \cdot \nabla\phi = -S(\phi) \tag{7.5}$$

7.2.1 Energy Equations

$$\nabla \cdot (\rho \mathbf{u} E) = \frac{1}{r}\frac{\partial}{\partial r}(r\rho u E) + \frac{\partial}{\partial z}(\rho w E) = -\frac{\partial F_k}{\partial z} \tag{7.6}$$

Multiplying equation 7.6 by r leads to equation 7.7.

$$r\nabla \cdot (\rho \mathbf{u} E) = \frac{\partial}{\partial r}(r\rho u E) + \frac{\partial}{\partial z}(r\rho w E) = -r\frac{\partial F_k}{\partial z} \tag{7.7}$$

Now we integrate over the annulus radially from r_i to r_o, and vertically from the sea surface to the top of the PBL, z_b.

$$\int_{r_i}^{r_o}\int_0^{z_b} r\nabla \cdot (\rho \mathbf{u} E) dz dr = \int_{r_i}^{r_o}\int_0^{z_b} -r\frac{\partial F_k}{\partial z} dz dr \tag{7.8}$$

Since we have assumed that the storm is axisymmetric, we do not need to consider any azimuthal variations. In addition, since the surface flux is only present at the lower boundary, the only contribution to the vertical integral is at $z = 0$, where $F_k = F_{k0}$. Since the integrals will be evaluated over narrow radial boxes, we can also assume that F_{k0} does not vary with radius. We thus achieve:

$$r_o\int_0^{z_b} \rho u E dz - r_i\int_0^{z_b} \rho u E dz + \int_{r_i}^{r_o} r\rho w E dr = \frac{1}{2}(r_o^2 - r_i^2)F_0 \tag{7.9}$$

For the next steps in the derivation, we would like to incorporate mass continuity into the equations so that the vertical motion does not explicitly appear. The mass continuity equation in cylindrical coordinates is shown in equation 7.10.

$$\frac{\partial}{\partial r}(r\rho u) + \frac{\partial}{\partial z}(r\rho w) = 0 \tag{7.10}$$

Integrating equation 7.10 over the depth of the boundary layer and from r_i to r_o produces equation 7.11, which can be seen to be similar in form to equation 7.9:

$$r_o \int_0^{z_b} (\rho u) dz - r_i \int_0^{z_b} (\rho u) dz + \int_{r_i}^{r_o} (r \rho w) dr = 0 \tag{7.11}$$

We now choose a value of total energy E_t so as to satisfy:

$$\int_{r_i}^{r_o} r \rho w E dr = E_t \int_{r_i}^{r_o} r \rho w dr \tag{7.12}$$

We now multiply equation 7.11 by the average value of total energy over the top edge of the annulus, E_t, and subtract it from equation 7.9, as shown in equation 7.13. This has the effect of removing the explicit vertical motion, since E_t times the third term of equation 7.11 is identically equal to the third term on the left-hand side of equation 7.9. Instead, the vertical flux is implicit in the difference between the two radial flux terms. The surface flux, on the right-hand side of the equation, has been expanded using the bulk aerodynamic formula. Here $|\mathbf{V_{10}}|$ is the magnitude of the 10m wind, k^* is the surface saturation enthalpy, and k is the 10m enthalpy.

$$r_o \int_0^{z_b} \rho u (E - E_t) dz - r_i \int_0^{z_b} \rho u (E - E_t) dz = \frac{1}{2} (r_o^2 - r_i^2) \rho C_k |\mathbf{V_{10}}| (k^* - k) \tag{7.13}$$

As with the drag coefficient, the value of the heat transfer coefficient will vary depending on the level at which it is evaluated. The standard altitude for C_d and C_k is 10m, but other altitudes can also be useful. Thus, an expression for C_k evaluated at the gradient wind level, C_{kGrad}, is shown below in equation 7.14; the advantage of these formulations is that only quantities at the top of the boundary layer are needed, instead of at the 10m level. This matches what is available in many models, and thus provides a more accurate way of calculating the heat flux than by parameterizing the low-level flow. Total energy is used instead of enthalpy, with the 10m wind speed used to calculate total energy at the surface (for E^*).

$$r_o \int_0^{z_b} \rho u (E - E_t) dz - r_i \int_0^{z_b} \rho u (E - E_t) dz = \frac{1}{2} (r_o^2 - r_i^2) \rho_{grad} |\mathbf{V_{grad}}| C_{kGrad} (E^* - E) \tag{7.14}$$

7.2.2 Entropy Equations

The budget of entropy can be examined using the value of $c_p ln(\theta_e)$, with $S(c_p ln(\theta_e)) = \frac{1}{T_s}\left(\frac{\partial F_k}{\partial z}\mathcal{D}\right)$, where T_s is the surface temperature, and $\mathcal{D}$ is the dissipative heating rate. The Joule heating term, H_d, the vertical integral of $\mathcal{D}$ over the depth of the boundary layer, is a source of entropy in this formulation.

$$\nabla \cdot (\mathbf{u}\rho c_p ln(\theta_e)) = -\frac{1}{T_s}\left(\frac{\partial F_k}{\partial z} + \mathcal{D}\right) \tag{7.15}$$

We follow a similar derivation as for total energy above, incorporating the vertical motion into the initial two terms. Integrating from the surface to the top of the boundary layer, z_b, and over the range of radii from outer, r_o to inner, r_i we get:

$$r_o \int_0^{z_b} \rho u c_p \left(\ln\theta_e - \ln\theta_{eT}\right) dz - r_i \int_0^{z_b} \rho u c_p \left(\ln\theta_e - \ln\theta_{eT}\right) dz = \frac{1}{2}(r_o^2 - r_i^2)\frac{F_{k0} + H_d}{T_s} \tag{7.16}$$

This leads to an equation for the transfer coefficient based on 10m conditions:

$$r_o \int_0^{z_b} \rho u c_p \left(\ln(\theta_e) - \ln(\theta_{eT})\right) dz - r_i \int_0^{z_b} \rho u c_p \left(\ln(\theta_e) - \ln(\theta_{eT})\right) dz = \frac{1}{2}(r_o^2 - r_i^2)\frac{\rho_0 \left(C_k|V|(k^* - k) + C_d|\mathbf{V_{10}}|^3\right)}{T_s} \tag{7.17}$$

For the calculation of the heat transfer based on gradient level winds and temperatures:

$$\begin{aligned} & r_o \int_0^{z_b} \rho u c_p \left(\ln(\theta_e) - \ln(\theta_{eT})\right) dz - \quad r_i \int_0^{z_b} \rho u c_p \left(\ln(\theta_e) - \ln(\theta_{eT})\right) dz \\ = \frac{1}{2}(r_o^2 - r_i^2)\frac{1}{T_s}\rho_{grad}(|\mathbf{V_{grad}}|C_k(E^* - E) & \quad + C_d|\mathbf{V_{grad}}|^3) \end{aligned} \tag{7.18}$$

7.3 Budget Values for each Storm

7.3.1 Floyd

For Hurricane Floyd, a value of 299.8K was chosen for the average SST; based on the AXBT values observed in the vicinity of the storm. For each experiment, the SST was also

specified to decrease towards the center, with a 1K drop between the outer edge and the center. This is to take into account the cooling due to mixing of the SST. Budgets of total energy and entropy were calculated, then the bulk aerodynamic formula was evaluated using observations from the 10m level and from the top of the boundary layer. This produces versions of C_k valid at 10m and 1000m respectively. As with the calculations for the drag coefficient, outliers for C_k below 0 and greater than 0.01 were excluded from the averaging. For Floyd, there were a number of negative outliers. Weighted means were calculated based on the full ensemble and also on the top 10% scored storm tracks. The results are summarized in Table 7.1.

Examination of the 10m values for C_k shows that the energy and entropy-derived values are in general agreement, and that the full ensemble average is consistent with the top 10% values. In aggregate, these calculations suggest that the value of C_k at 10m for Floyd is a bit less than 0.0010. This is fairly close to the value of 0.00113 found by Large and Pond (1982), though that study was for much lighter winds.

The gradient level values of C_k were calculated using both energy and entropy budgets. The radial heat flux used is the same as for the 10m values, but the values of wind speed, and density in the bulk aerodynamic formula are those observed at the top of the boundary layer. In addition, instead of using the difference between the saturated enthalpy at the sea surface and the observed enthalpy at 10m, this calculation uses the saturated total energy of the sea surface and the observed total energy at the top of the boundary layer. The gradient level wind is used at the surface as well as for the observed value of total energy. This form is used because the decrease in temperature with height is not accounted for in enthalpy. The aggregate of the values of C_k at the gradient level is about 0.0008. The top 10% scored values show more variation – the entropy and the energy versions are smaller than the mean of the whole ensemble. Since the gradient level winds are significantly stronger than the 10m winds, the gradient level C_k values are somewhat smaller than the 10m values. Since the top 10% scored values represent the best tracks analyzed, these should be taken as more representative numbers; thus the C_k values at gradient level for Floyd work out to be around 0.0005.

Quantity	Mean Value	Standard Deviation
10m C_k	0.0015	0.0017
10m $C_{k\theta}$	0.00099	0.0065
Top 10% 10m C_k	0.00083	0.00085
Top 10% 10m $C_{k\theta}$	0.00089	0.00049
Gradient C_k	0.0012	0.0014
Gradient $C_{k\theta}$	0.0011	0.0021
Top 10% Gradient C_k	0.00054	0.00047
Top 10% Gradient $C_{k\theta}$	0.00039	0.00027

Table 7.1: Heat Transfer Coefficient Values for Floyd

Quantity	Mean Value	Standard Deviation
10m C_k	0.00067	0.00064
10m $C_{k\theta}$	0.00076	0.00097
Top 10% 10m C_k	0.00092	0.00060
Top 10% 10m $C_{k\theta}$	0.0010	0.00063
Gradient C_k	0.00037	0.00037
Gradient $C_{k\theta}$	0.00034	0.00036
Top 10% Gradient C_k	0.00052	0.00033
Top 10% Gradient $C_{k\theta}$	0.00042	0.00033

Table 7.2: Heat Transfer Coefficient Values for Georges

7.3.2 Georges

A SST of 301K (28°C) was used to calculate the heat budget for Georges, based on observations from AXBTs. Values of all versions of C_k were close to those derived for Floyd. The values of C_k for Georges are shown in Table 7.2. There was less variation between the full mean and the top 10% scored means than for Floyd, but the top 10% scores show better agreement with the Floyd values. They also have smaller standard deviations, which gives more confidence in the values. For the 10m level, the top 10% values for C_k are around 0.001, and at the gradient level, the top 10% values are around 0.0005. An examination of the plot of all C_k values indicates a trend toward larger values with better scores; negative values are mostly reported with the poorest scoring tracks.

Quantity	Mean Value	Standard Deviation
10m C_k	0.00091	0.0010
10m $C_{k\theta}$	0.0010	0.0017
Top 10% 10m C_k	0.00068	0.00071
Top 10% 10m $C_{k\theta}$	0.00093	0.00085
Gradient C_k	0.00048	0.00060
Gradient $C_{k\theta}$	0.00050	0.00067
Top 10% Gradient C_k	0.00037	0.00037
Top 10% Gradient $C_{k\theta}$	0.00038	0.00043

Table 7.3: Heat Transfer Coefficient Values for Mitch

7.3.3 Mitch

For Mitch, AXBTs showed SSTs of around 28-29C in the area of the storm, but the storm spent a long period of time over the same area, so it is likely that mixing effects served to lower the sea surface temperature, especially towards the center of the hurricane. Dropsondes recorded air temperatures just above the surface in the eyewall in the range of 24C; this combination of evidence leads to choosing a cooler SST than the original estimates. The budget calculations were run using a SST of 299K (25.85^oC).

The coefficient values for Mitch, shown in Table 7.3, were the lowest of all three storms. A possible explanation for this is that actual sea surface temperatures could have been even cooler than the value chosen. Mitch had begun a slow weakening at the time of the dropsonde observations, after having been a category 5 storm. The most likely explanation for the decrease in intensity is that surface heat fluxes began to diminish; cooling of the oceanic mixing layer due to turbulent entrainment being the main source of this change.

The aggregate values of 10m C_k are around 0.00010; the aggregate gradient level C_k is about 0.0007. These values are in line with the values for Floyd and Georges. There is only a small difference between the energy and entropy versions of C_k for Mitch.

7.4 Summary

For all three storms, the energy and entropy budgets yielded values that were fairly similar, as shown in Table 7.4. Thus, to compute an average value of C_k, both the energy and entropy budget results are used. For the 10m value of C_k, the mean is 0.00088. For the

Quantity	Mean Value	Standard Deviation
Floyd 10m C_k	0.00083	0.00085
Floyd 10m $C_{k\theta}$	0.00089	0.00049
Georges 10m C_k	0.00092	0.00060
Georges 10m $C_{k\theta}$	0.0010	0.00063
Mitch 10m C_k	0.00068	0.00071
Mitch 10m $C_{k\theta}$	0.00093	0.00085
Floyd Gradient C_k	0.00054	0.00047
Floyd Gradient $C_{k\theta}$	0.00039	0.00027
Georges Gradient C_k	0.00052	0.00033
Georges Gradient $C_{k\theta}$	0.00042	0.00033
Mitch Gradient C_k	0.00037	0.00037
Mitch Gradient $C_{k\theta}$	0.00038	0.00043

Table 7.4: Heat Transfer Coefficient Values

gradient level value of C_k, the mean is 0.00044. These values are significantly smaller than those determined by Large and Pond (1982), which were also for lighter wind conditions. For a hurricane to maintain itself, we expect that larger fluxes are needed than those shown here; a mechanism for this will be suggested in the next chapter.

Chapter 8

Vertical Eddy Heat Fluxes

8.1 Budget Equation with Eddy Terms

Calculations of the energy and entropy budgets earlier in this paper are based on the mean values of the flow and thermodynamic fields. In an ideal case, a hurricane eyewall can be thought of as having nearly constant entropy or total energy with height. If this were true, then eddy fluxes would not be an important term in the budgets. Variations from this state, though, would allow the development of updrafts and downdrafts which could lead to a net upward transport of energy and entropy out of the boundary layer. Thus, we will here attempt to account for the effects of vertical eddy fluxes of entropy and energy. In order to accomplish this, the vertical fluxes can be split into mean and perturbation values. Thus, we have $w = \overline{w} + w'$ for vertical velocity, $\ln\theta_e = \overline{\ln\theta_e} + \ln\theta_e'$ for entropy, and $E = \overline{E} + E'$ for total energy.

$$\nabla \cdot (\rho \mathbf{u} E) = \frac{1}{r}\frac{\partial}{\partial r}(r\rho u E) + \frac{\partial}{\partial z}(\rho w E) = -\frac{\partial F}{\partial z} \tag{8.1}$$

$$r\nabla \cdot (\rho \mathbf{u} E) = \frac{\partial}{\partial r}(r\rho u E) + \frac{\partial}{\partial z}(r\rho w E) = -r\frac{\partial F}{\partial z} \tag{8.2}$$

Expanded to include vertical eddy fluxes, Equation 8.2 becomes:

$$r\nabla \cdot (\rho \mathbf{u} E) = \frac{\partial}{\partial r}(r\rho u E) + \frac{\partial}{\partial z}(r\rho \overline{w}\overline{E}) = -r\frac{\partial F}{\partial z} \tag{8.3}$$

Now integrate over the annulus from r_i to r_o, and from the sea surface to the top of PBL, z_b.

$$\int_{r_i}^{r_o}\int_0^{z_b} r\nabla\cdot(\rho\mathbf{u}E)dzdr = \int_{r_i}^{r_o}\int_0^{z_b} -r\frac{\partial F}{\partial z}dzd\theta dr \tag{8.4}$$

Instead of assuming that eddy fluxes are zero at the top of the boundary layer, as we did in equation 7.17, we will retain that term and evaluate it using aircraft measurements.

$$r_o\int_0^{z_b}\rho uEdz - r_i\int_0^{z_b}\rho uEdz + \int_{r_i}^{r_o} r\rho\overline{w}\overline{E}dr = \frac{(r_o^2-r_i^2)}{2}F_0 - \int_{r_i}^{r_o} r\rho w'E'dr \tag{8.5}$$

$$r_o\int_0^{z_b}\rho uEdz - r_i\int_0^{z_b}\rho uEdz + \int_{r_i}^{r_o} r\rho\overline{w}\overline{E}dr = \frac{(r_o^2-r_i^2)}{2}\rho|\mathbf{V_{10}}|C_k(k^*-k) - \int_{r_i}^{r_o} r\rho w'E'dr \tag{8.6}$$

Similarly for entropy:

$$\begin{aligned} & r_o\int_0^{z_b}\rho uc_p\ln(\theta_e)dz \quad - r_i\textstyle\int_0^{z_b}\rho uc_p\ln(\theta_e)dz \quad + \int_{r_i}^{r_o} r\rho c_p\overline{w}\overline{\ln\theta_e}dr \\ = \frac{(r_o^2-r_i^2)}{2T_s}\rho(|\mathbf{V_{10}}|C_k(k^*-k) + C_d|\mathbf{V}|^3) & \quad - \textstyle\int_{r_i}^{r_o} r\rho c_p w'(\ln\theta_e)'dr \end{aligned} \tag{8.7}$$

8.2 Determination of Eddy Fluxes

Vertical eddy transport can be shown to play an important role in the budgets of entropy and energy. By eddy transport, we refer to the motions that are not resolved by the averaged values calculated for each grid box. The flight and dropsonde observations were composited so that each grid box was 60km wide in potential radius; thus averaging was performed azimuthally, in time, and over the width of the box. Therefore, any features that were not large and persistent would be smoothed. The first order features of the hurricane, such as the rising motion in the eyewall, are clearly resolved. However, it is likely that smaller scale or shorter duration patterns could also contribute to the heat and entropy budget.

These updrafts and downdrafts can have the effect of enhancing transport of energy and entropy on top of the transport due to the mean flow. Convective updrafts will have relatively higher values of energy and entropy as well as positive perturbation vertical velocities. The downdrafts will tend to be cooler and drier, with consequent lower values of E and θ_e, with negative vertical velocities.

We calculated vertical eddy fluxes of entropy and total energy using the data provided by the aircraft flights – the aircraft observed the thermodynamic parameters as well as the vertical motion. A mean state of energy and entropy was calculated, which included the trend of the data's variation with potential radius. The perturbations were calculated from the deviation of individual observations from this trendline.

8.3 Results

For Floyd, the mean vertical eddy flux ($ln\theta_e'w'$) over all flight-level observations was 0.0019 m/s. In the eyewall region, the eddy entropy flux was 0.0021 m/s. For total energy ($E'w'$) the mean over all observations was 610 m^3s^{-3} and over the eyewall region it was 700 m^3s^{-3}.

For Georges, the mean vertical eddy flux ($ln\theta_e'w'$) over all observations was 0.0033 m/s. In the eyewall region, the eddy entropy flux was 0.0045 m/s. For total energy ($E'w'$) the mean over all observations was 1000 m^3s^{-3} and over the eyewall region it was 1400 m^3s^{-3}. Much stronger local updrafts were measured in Georges; these most likely contributed to the higher values than those for Floyd.

For Mitch, the mean vertical eddy flux ($ln\theta_e'w'$) over all observations was -0.0012 m/s. In the eyewall region, the eddy entropy flux was -0.0016 m/s. For total energy ($E'w'$) the mean over all observations was -240 m^3s^{-3} and over the eyewall region it was -370 m^3s^{-3}. When compared to the eddy fluxes for Georges and Floyd, those for Mitch are somewhat smaller in magnitude and also negative.

We can see from equations 8.6 and 8.7 that the contribution to C_k from the eddy flux can be expressed as:

$$\Delta C_k = \frac{\rho_{top} w' E'}{\rho_0 |\mathbf{V_{10}}| (k^* - k)} \tag{8.8}$$

Parameter	Calculated Value
ρ_0	1.1 kg/m^3
V_{10}	40 m/s
$(k^* - k_{10})$	10000 J/kg
$w'E'$	700 $m^3 s^{-3}$
Energy ΔC_k	0.0018
T_s	300K
$w' \ln \theta_e'$	0.0021 ms^{-1}
Entropy ΔC_k	0.0014
V_{grad}	60 m/s
Gradient Energy ΔC_k	0.0012
Gradient Entropy ΔC_k	0.0010

Table 8.1: Estimate of vertical eddy heat flux for Floyd

$$\Delta C_k = \frac{\rho_{top} T_s c_p w' \ln \theta_e'}{\rho_0 |\mathbf{V_{10}}| (k^* - k)} \tag{8.9}$$

where ρ_{top} is the density at the top of the boundary layer.

Using equations 8.8 and 8.9, we can estimate the magnitude of the eddy heat and entropy fluxes for each storm. The values of w', E', and $\ln \theta_e'$ were calculated as the deviations from the average values over the 60km potential radius grid boxes. The flight-level observations are provided in bins that contain weighted values over 2km in physical radius space, so any features smaller than that scale may not be resolved in these computations. The flight levels are 650mb and 700mb, which is above the top of the boundary layer.

While the large-scale upward motion of the hurricane is not a result of convective instability, the presence of downdrafts suggests that there is some unsaturated air present somewhere in the vertical column. This can be thought of as a manifestation of some convective available potential energy (CAPE) in the system – this is not the main energy source for the hurricane, but may be a factor in the heat and entropy budgets. A warm, moist, rising parcel of air would then begin to accelerate with height through the region of positive CAPE; in general, we would expect that the velocity would be greater at 700mb than at the top of the boundary layer. From these considerations, it seems likely that the vertical eddy fluxes at the top of the boundary layer would be somewhat smaller than those observed by the aircraft at the 700mb level.

ρ_0	1.1 kg/m^3
V_{10}	50 m/s
$(k^* - k_{10})$	12000 J/kg
$w'E'$	1400 m^3s^{-3}
Energy ΔC_k	0.0021
T_s	301K
$w' \ln \theta'_e$	0.0045 ms^{-1}
Entropy ΔC_k	0.0021
V_{grad}	70 m/s
Gradient Energy ΔC_k	0.0015
Gradient Entropy ΔC_k	0.0015

Table 8.2: Estimate of vertical eddy heat flux for Georges

ρ_0	1.1 kg/m^3
V_{10}	40 m/s
$(k^* - k_{10})$	7000 J/kg
$w'E'$	-370 m^3s^{-3}
Energy ΔC_k	-0.0012
T_s	299K
$w' \ln \theta'_e$	-0.0016 ms^{-1}
Entropy ΔC_k	-0.0016
V_{grad}	60 m/s
Gradient Energy ΔC_k	-0.0008
Gradient Entropy ΔC_k	-0.0010

Table 8.3: Estimate of vertical eddy heat flux for Mitch

The observed values used to estimate eddy fluxes for all three storms are provided in tables 8.1, 8.2, and 8.3. We can see from these scaling estimates that the eddy flux is the same magnitude as the flux calculated from the mean flow for the Floyd and Georges cases. The eddy flux was quite variable between storms, however. For Mitch, the mean eddy flux values are of similar magnitude, but are negative. Also for Mitch, the means appear to be strongly influenced by a group of observations of very strong downdrafts ($> 7\ ms^{-1}$) which have large negative values of $w' \ln \theta'_e$.

These differences are likely the result of the stage in development of the hurricane; Georges had the highest values, and had just completed a sharp intensification at the time of the observations. Floyd was just past peak intensity but remained a strong hurricane with concentric eyewalls. Mitch was past its peak intensity, and continued to weaken due in part to its slow motion which left it over cooling ocean waters. Convection was likely less vigorous under these conditions, and there was probably less vertical gradient of energy and entropy for downdrafts to work from. Since the eddy flux contribution to C_k for Mitch is negative and of larger magnitude than that of the budget-derived C_k, we will not further examine the combined value of C_k, as its negative value is not physically meaningful. Most likely, a budget that matched the top of the boundary layer with the observations of eddy flux would give a positive value of C_k. The important effect of a few strongly descending downdrafts may also be non-representative of the average environment of the storm.

8.4 Summary

Vertical eddy flux of energy and entropy plays a significant effect in the hurricane eyewall. For both budgets, the eddy contribution is on the same order of magnitude as the flux calculated using mean vertical transport. The only data available with appropriate resolution are from 650mb and 700mb; we expect that eddy fluxes would be somewhat smaller at the top of the boundary layer. The change to C_{kGrad}, the gradient level C_k, is somewhat smaller than the 10m values indicated in the tables, due to the stronger windspeeds at the top of the boundary layer.

Chapter 9

Calculations of the Ratio $\frac{C_k}{C_d}$

9.1 Equations for Calculating the Coefficients

9.1.1 Curve-Fitting of Points by R

One approach for calculating the exchange coefficients is to use the formulations from Bister and Emanuel (1997) to determine the ratio of C_d/C_k. A few approaches may be tried – it can be shown that the ratio is dependent on various expressions for the temperature or energy of the air in the storm and at the sea surface. Below are the equations for this ratio, based on total energy. Note that the sea surface value of total energy is also required; this is calculated by using the sea surface temperature instead of an air temperature, a relative humidity of 100%, with the rest of the parameters taking their values at the lowest level. For the wind speed needed for total energy, the value is chosen as the gradient wind at the top of the boundary layer.

The curve fitting routine used to determine the constants is quite dependent on the value of E^*. An analytical expression for the ratio of C_k/C_d can be obtained as follows, starting with equations for wind stress and enthalpy flux from Bister and Emanuel, 1998:

$$\int \rho u \frac{\partial M}{\partial r} dz = -r C_d \rho_0 |V| V_t \tag{9.1}$$

$$\int \rho u \frac{\partial E}{\partial r} dz = C_k \rho_0 |V| (k_o^* - k) \tag{9.2}$$

If we assume that E and M are functions only of each other, we can get the following expression relating the two.

$$\frac{dE}{dM} = -\frac{C_k}{C_d}\frac{(k_o^* - k)}{rV_t} \approx -\frac{C_k}{C_d}\frac{(E_o^* - E)}{rV_t} \tag{9.3}$$

Expand out M, taking advantage of the fact that in the eyewall $rV_t \approx M = \frac{1}{2}fR^2$:

$$R\frac{dE}{dR} = -2\frac{C_k}{C_d}(E_0^* - E) \tag{9.4}$$

Rearranging yields:

$$R\frac{dE}{dR} - 2\frac{C_k}{C_d}E = -2\frac{C_k}{C_d}E_0^* \tag{9.5}$$

If we make the assumption that E_0^* is constant (which examination of the data bears out fairly well), we can phrase the relation as an exponential function of R. A budget of entropy cannot be phrased in an equation as simple as this, because a term for dissipative heating must also be included. Thus we will just work with the energy equation.

$$E = E_0^* - AR^{2\frac{C_k}{C_d}} \tag{9.6}$$

Since the goal of this derivation is an equation that a line can be fit to, we take the logarithm so that it becomes a linear equation, where A is an integration constant.

$$ln(E_0^* - E) = ln(A) + 2\frac{C_k}{C_d}ln(R) \tag{9.7}$$

We can then use a linear least-squares algorithm to compute the best fit to observations.

9.1.2 Sounding – Boundary Layer Averages

By averaging the values of E and R for each sounding over the depth of the boundary layer (before compositing data) we can produce a set of observations for curve-fitting to equation 9.7. Note that the form of this equation causes the line to have an R intercept at E_0^*, so along with using the least squares algorithm to estimate A and $\frac{C_k}{C_d}$, a separate loop attempting various values of E^* is also performed. The curve-fit that has the highest correlation coefficient is selected as the best fit.

9.1.3 Calculation of Ratio on Individual Flight Legs

The plots of sounding data reveal that total energy remains nearly constant with altitude along potential radius surfaces (inside the eyewall), which is what we would expect given a regime of slantwise convective neutrality. This appears to be consistent up to flight level of 650mb or 700mb, so we can use the values obtained from the aircraft data to calculate the ratio of exchange coefficients.

A useful feature of the flight-level data is that is is an inbound or outbound pass, from the center out as far as a few hundred kilometers. This data then has a horizontal coherence that is not always available from the composited soundings. For calculating the ratio of C_k/C_d, we can make use of these passes even for storms that are not completely symmetric. We make the assumption that since the eyewall is the site of vigorous convection, the conserved thermodynamic variables ought to retain the same values at flight level as they had at the surface. Examination of the flight level data shows that in the eyewall region, most observations are very close to saturation (relative humidity 95%), which is consistent with that assumption.

Note that the full budget equations to calculate C_d and C_k separately would not make sense if applied to flight level. This is because we expect that the radial inflows of angular momentum and heat are being balanced with the surface fluxes. Thus the radial velocity at the surface is crucial; the flight-level radial velocity is not representative of the surface value. In fact, we have used a constraint attempting to minimize radial velocities at flight level to determine the best track. Nevertheless, we expect that total energy at this level corresponds to the surface value, due to the strong upward velocities experienced in the eyewall.

9.1.4 Cartesian Distribution of total energy and θ_e For Storms

A factor that led to the adoption of the single flight analysis technique was that for some storms, distributions of total energy and θ_e were not azimuthally uniform. Figure 9-1 shows the Cartesian distribution of boundary layer θ_e for Georges, in the transformed potential radius distances, derived from dropsonde data. The distribution of total energy is similar; θ_e will be analyzed to emphasize how much temperature and humidity vary across the domain,

while excluding the effect of windspeed. The expected gross trend of higher values toward the center is observed, but there is much small-scale variability present. This is not all due to the time compositing. Note the observations in the lower right corner, at 2329Z and 2338Z. While both are at about the same potential radius from the center, θ_e is different between the two by 6K. Another example is in the center-right portion of the diagram; observations at 1933Z and 2254Z. Here, an observation 6K cooler is located 200 km (potential radius) closer to the center. These types of deviations from the predicted structure of the storm serve to make calculation of the heat budget error-prone. Notes included with the sounding data indicate problems with the humidity sensors for many drops (though not with the 4 sondes just identified). The 1933Z sonde shows saturated conditions, but a surface temperature of 23.74C. The 2338Z sonde shows 74% relative humidity and 28.12C at the surface, with unsaturated conditions over the depth of the sounding from 7000m down. The 2329Z sonde shows 86% relative humidity and 27.02C at the surface, but saturated above 900m. The 2254Z sonde shows 28.50C and 83.0% relative humidity, unsaturated from the surface to 6700m. Thus we can have quite different values composited close together in space; this makes curve-fitting imprecise.

9.1.5 Error Sensitivity

There are a number of ways that error could have been introduced into the data used for these calculations. There are errors due to instrument error, both for atmospheric and SST measurements, and errors due to analyzing the location of the measurement. Since we are using the potential radius, this location error also incorporates error in tangential velocity. The radial and tangential components of wind have a few sources of error. First, there is the measurement error of the dropsonde or on the flight. Then there is error due to how u and v components of the wind are assigned to radial and tangential. For the dropsondes, the winds have been adjusted to be storm relative; this means that any errors in the propagation speed of the storm would go into the u and v winds. For the flight-level winds, the dataset from HRD comes already in radial and tangential components, with the storm motion removed; presumably they have applied the same process of removing the storm motion from the observed winds.

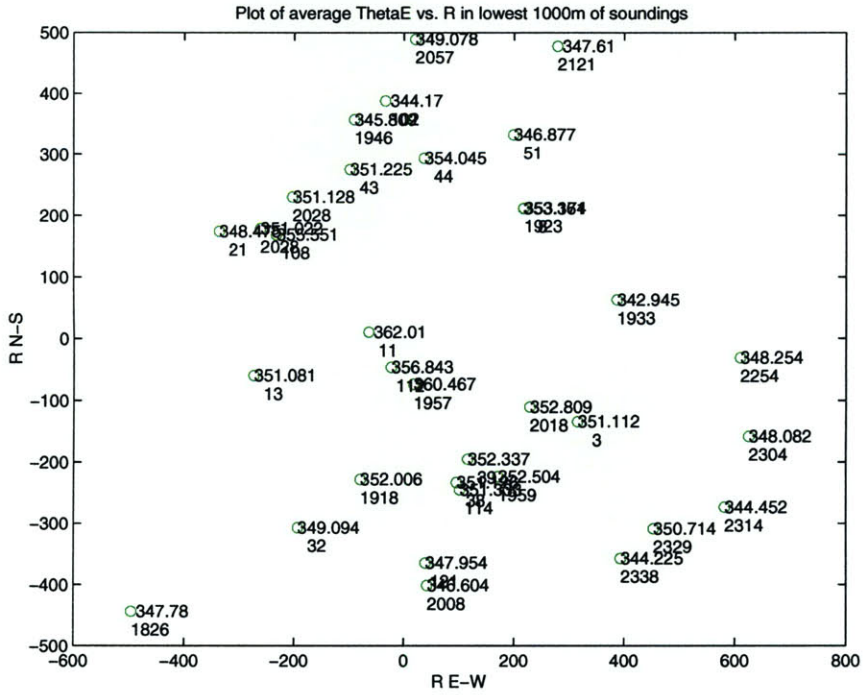

Figure 9-1: Cartesian plot of θ_e for Georges, with times

Storm	SST	Central Pressure	V_{max}	θ_e	E
Floyd	299.8	925 mb	63	369.6	65285
Georges	301	940 mb	67	372.8	70086
Mitch	299	926 mb	66	365.7	61862
Mitch	301.6	926 mb	66	378.3	73852

Table 9.1: Values for calculating E^* and θ_e^*

The values for equivalent potential temperature and total energy have a number of sources of error. Temperature and humidity measurement errors are obvious sources. For total energy, the wind speed and all of the uncertainties mentioned above plays a part. For the sounding data, the θ_e and total energies are averaged over the lowest 1000m of the storm; the standard deviation of the values in this average must also be examined.

9.2 Results

9.2.1 Floyd

Boundary Layer Ratio Calculation

For Floyd, the quality of the composite was good, so we can make use of the formula for calculating the ratio of the coefficients using the surface values. This calculation was performed by allowing the values of E* to be varied, then rating the fit by the correlation coefficient. Graphs of the sensitivity to the sea surface temperature are also provided in Figures 9-2, and 9-3. In these figures, a vertical line is displayed at the location of the highest observed value of E; equation 9.7 can be seen to have no solution if one of the observation values is identical to E_0^*. Thus, close to this limit, the curve-fitting algorithm is approaching a singularity, and behaves oddly. Ideally, we would expect that values of E should be close to, but smaller than E_0^*.

For E*, a value of 61584 J/kg is chosen; this gives a correlation of 0.8947 and a ratio of C_k/C_d of 0.63. The curve is shown in Figure 9-4. The average SST measured by AXBT for Floyd was 300.6K, and a minimum pressure of 925mb was recorded by dropsonde. If an SST of 299.8K is used, under the assumption that the center has cooled somewhat due to deepening of the mixing layer, we get values of $\theta_e^* = 369.6$K and E^* of 65285 J/kg. Thus, a somewhat lower value of E^* than the computed value yields the best correlation.

Flight Level Ratio Calculation

The flight level data for Floyd was used to try to fit to the exponential expression for C_k/C_d. Figure 9-5 shows the values of E observed by the aircraft, as well as the saturation surface value of E, E^*, calculated using the SST, pressure at the given radius, and the maximum windspeed for the sounding. Nearly all of the flight level observations in the eyewall are at or close to saturation, so E does not vary significantly from E^*. An interesting feature is that the maximum value of E^* is not observed close to the center, where pressure is lowest, but rather at the radius of maximum winds. The distribution of E^* with potential radius, also shows that the variations are not large, when compared to the observed flight level values. Thus, an assumption of constant E^* with radius is not unwarranted.

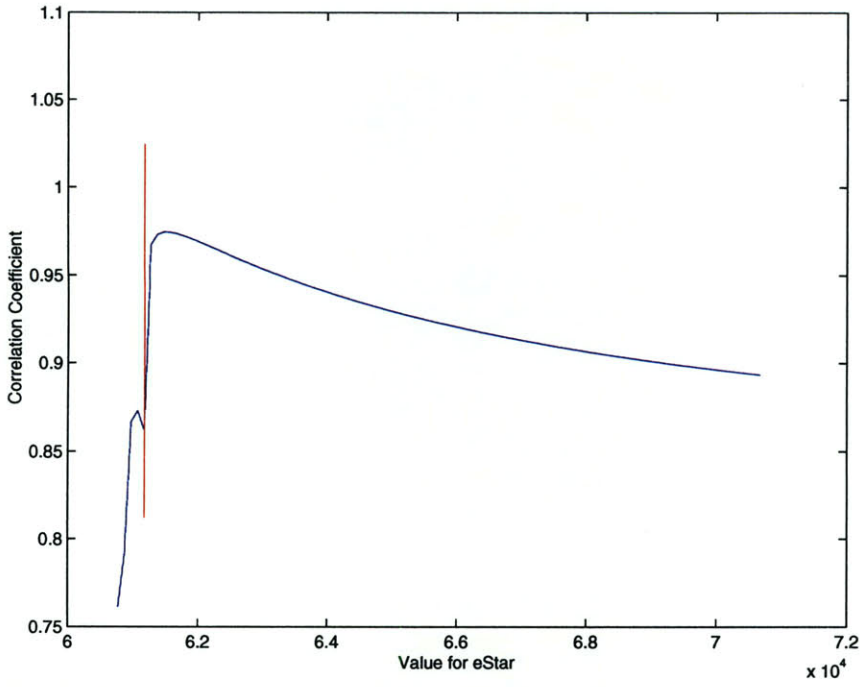

Figure 9-2: E* vs. Correlation Coefficient for Floyd

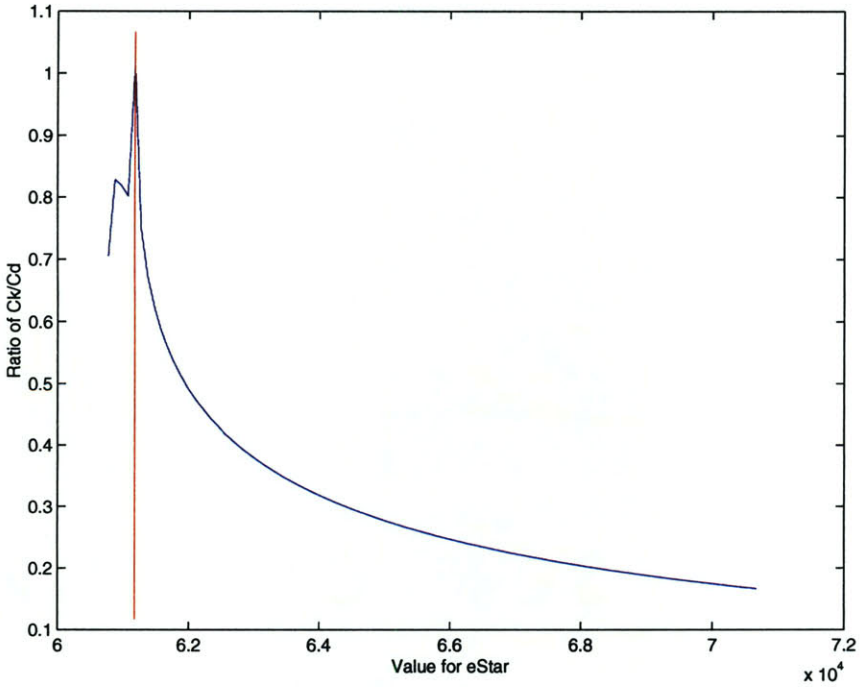

Figure 9-3: E* vs. Ratio of C_k/C_d for Floyd

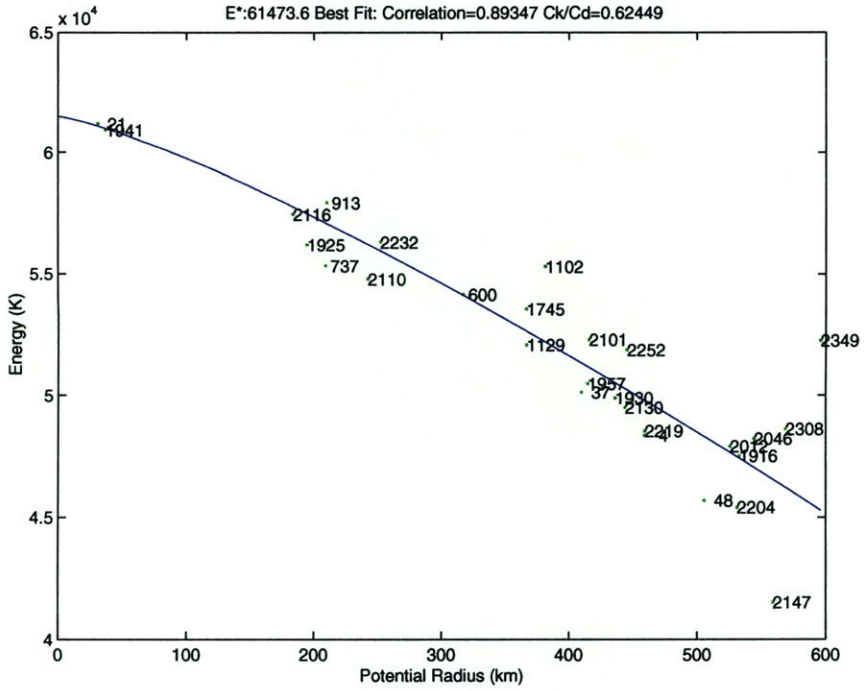

Figure 9-4: Best fit to observations for E for Floyd

Figures 9-6 and 9-7 show the dependence of the correlation coefficient and C_k/C_d ratio on the value of E_0^*. Figure 9-6 shows that the correlation coefficient remains nearly constant at about 0.76 for $E_0^* > 65000$. Figure 9-7 shows that for E_0^* from 65000 to 70000 the ratio of C_k/C_d declines from 0.42 to 0.30. Since the correlation coefficient is similar over this entire range, the range of values for the ratio must be considered as equally likely. The observed values of E^* are around 65000, leading to a ratio value of 0.42.

Figure 9-8 shows the curve fit at the best correlation. The scatter of the flight-level E values is fairly large at any radius, and the individual flights also show much small-scale variation.

9.2.2 Georges Flight Level Data

The sea surface saturation value of θ_e, at 940mb and 301K, is 372.84K. If we fit the flight level data to a curve based on that value, we find that some profiles contain regions of θ_e up to of 375K. If the maximum sea surface value is indeed as specified, this means that other factors are at work. Emanuel, 1995, shows that convection alone cannot cause temperatures

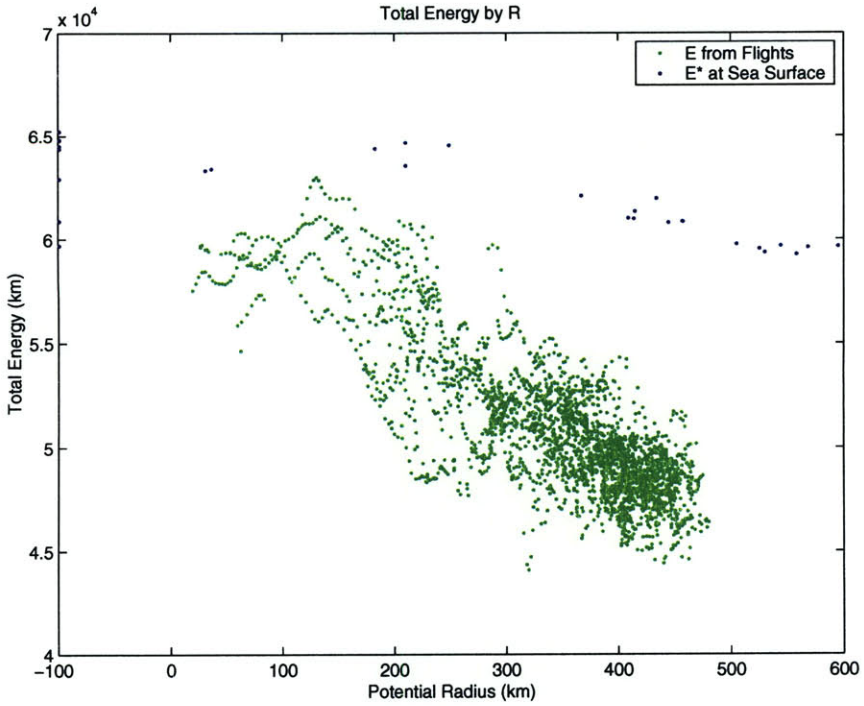

Figure 9-5: Flight Level E values vs. R for Floyd

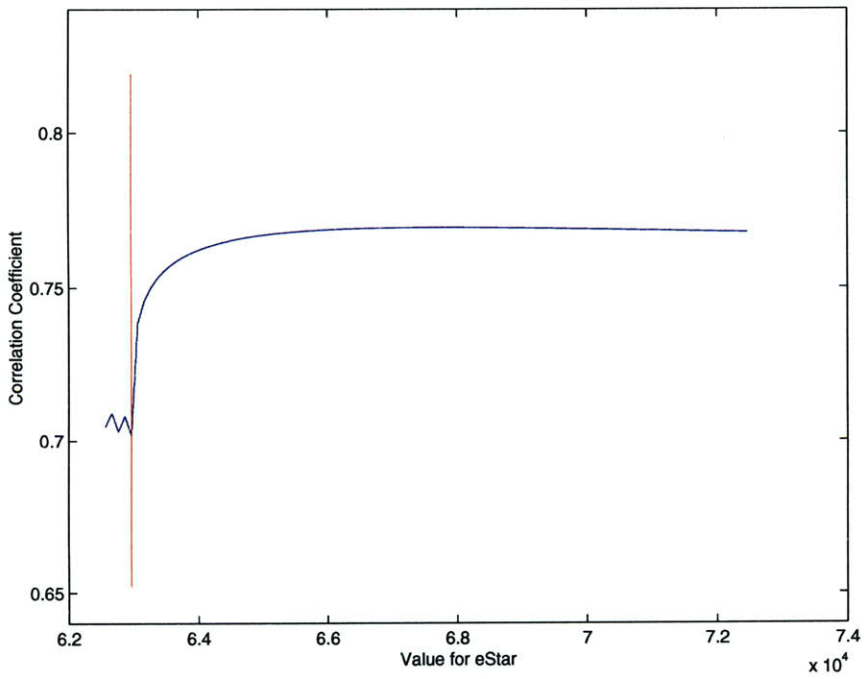

Figure 9-6: E* vs. Correlation Coefficient for Floyd

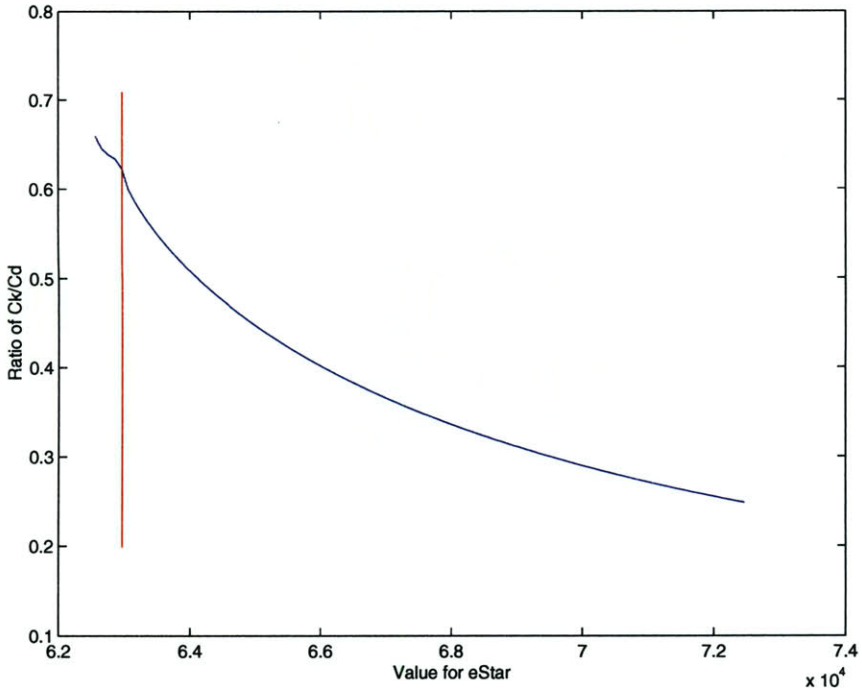

Figure 9-7: E* vs. Ratio of C_k/C_d for Floyd

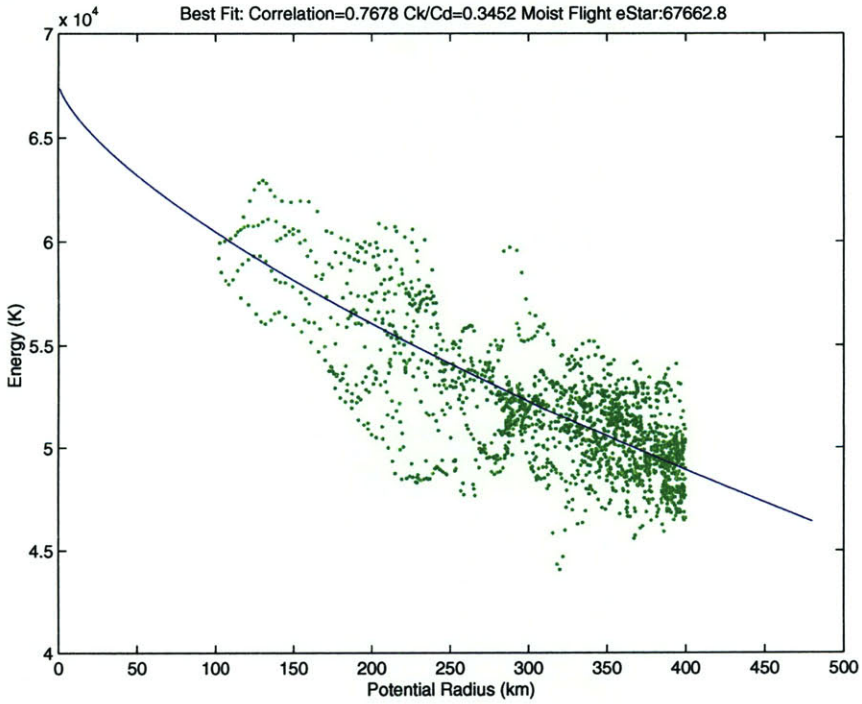

Figure 9-8: Best fit to observations for E for Floyd

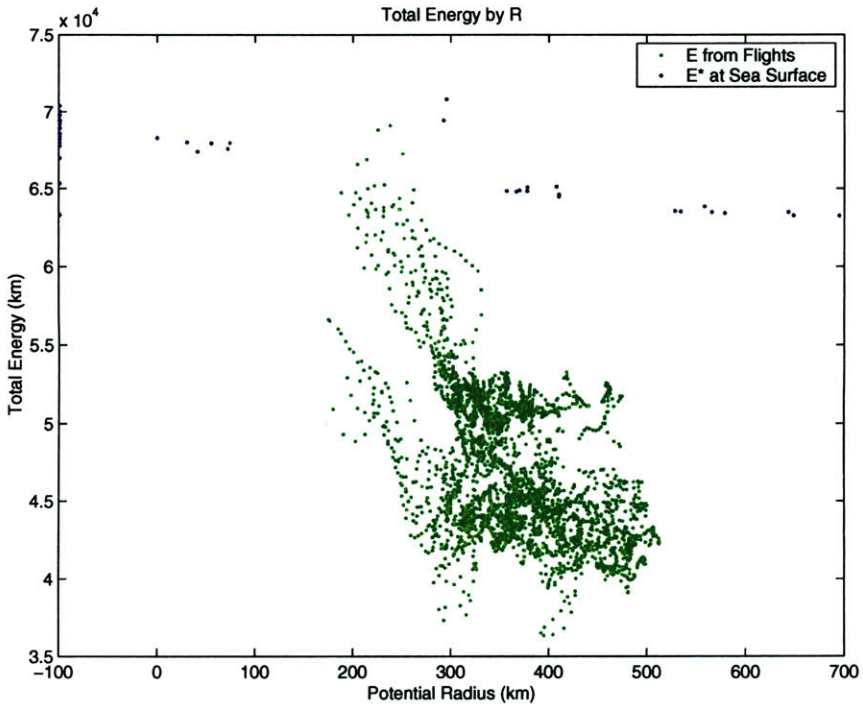

Figure 9-9: Flight Level E values vs. R for Georges

to exceed that of the convective updrafts. One possibility is that the parameters used to choose that value are incorrect; perhaps the SST is somewhat warmer in parts of the storm, or the central pressure is lower. Instrument error or bias is also a possibility. Frictional dissipation may also be a source of this heating.

Figure 9-9 shows the values of total energy observed at flight level, and the values of sea surface saturation total energy, E^*. The interesting feature of this plot is that the E^* value is always greater that the value of E. This suggests that the source of the heating to cause θ_e values larger than θ_e^* is indeed the contribution of the wind kinetic energy; i.e. dissipative heating.

Figures 9-10 and 9-11 show the dependence of the correlation coefficient and C_k/C_d ratio on the value of E_0^*. Figure 9-10 shows that the correlation coefficient remains nearly constant at about 0.48 for $E_0^* > 70000$, declining very slowly with higher E^*. Figure 9-11 shows that for E_0^* from 70000 to 75000 the ratio of C_k/C_d declines from 0.54 to 0.38. Based on the AXBT observed sea surface temperatures, the maximum value of E^* is about 70000; this would imply a ratio of around 0.54.

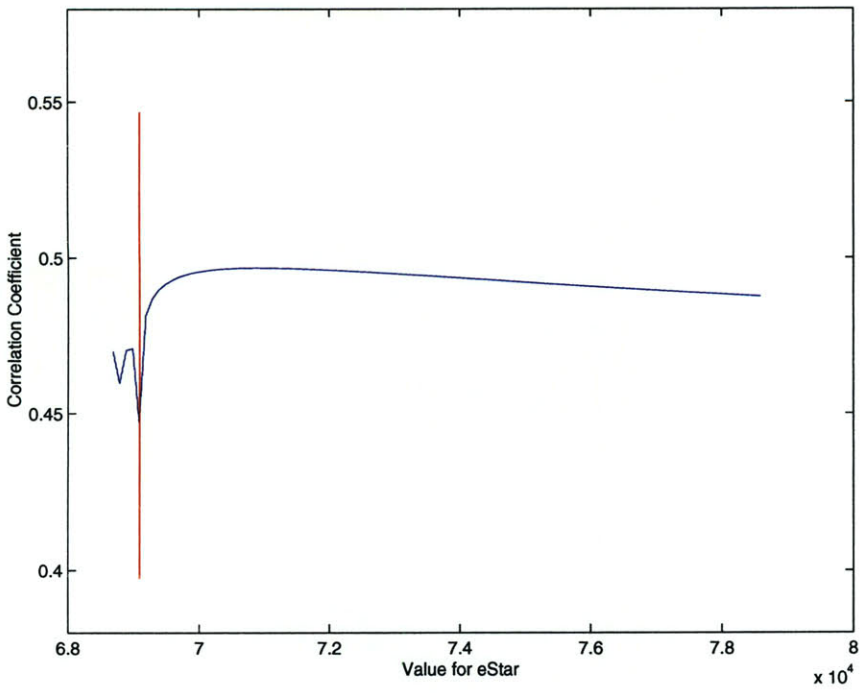

Figure 9-10: E* vs. Correlation Coefficient for Georges

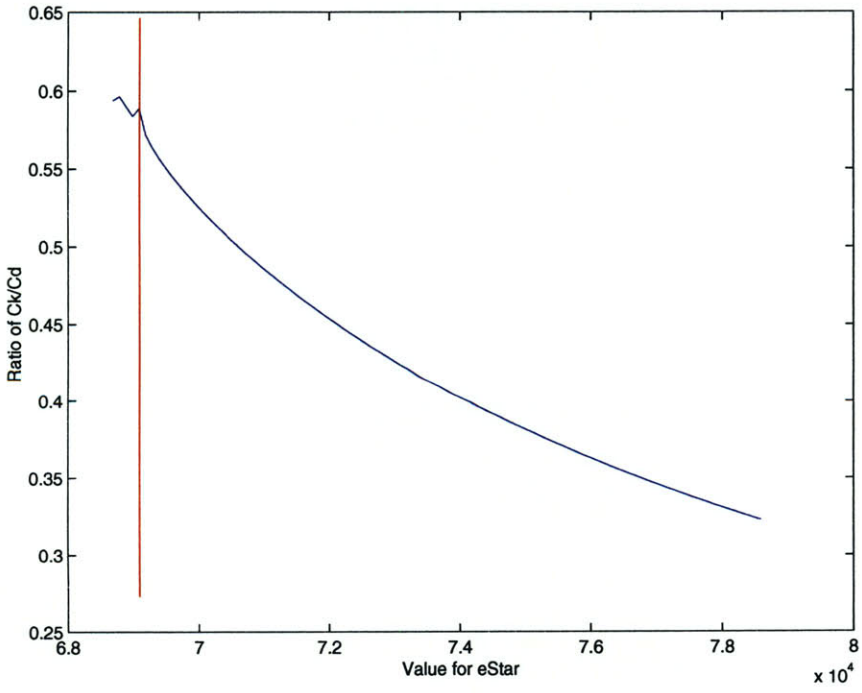

Figure 9-11: E* vs. Ratio of C_k/C_d for Georges

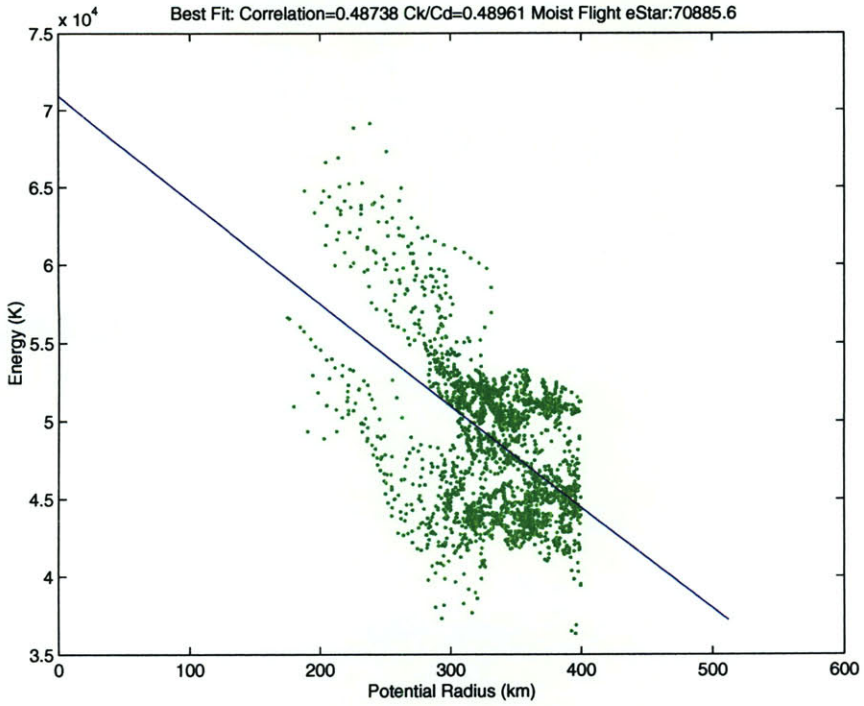

Figure 9-12: Best fit to observations for E for Georges

9.2.3 Mitch Flight Level Data

Figures 9-14 and 9-15 show the dependence of the correlation coefficient and C_k/C_d ratio on the value of E_0^*. Figure 9-14 shows that the correlation coefficient remains nearly constant at about 0.55 for $E_0^* > 72000$. Figure 9-15 shows that for E_0^* from 72000 to 77000 the ratio of C_k/C_d declines from 0.30 to 0.22. Based on the AXBT observed sea surface temperatures of 301.6K, the maximum value of E^* is about 74000; this would imply a ratio of around 0.25.

9.3 Comparison with Budget Values

If we note that all of the storms had similar wind speeds, we can consider an average value of the C_k/C_d ratio based on all three hurricanes. The mean ratio from the budget calculations is 0.29 ± 0.089 and the mean ratio from the flight-level (plus boundary layer ratio for Floyd of 0.62) data is 0.46 ± 0.16. The budget ratios for Floyd and Georges had some differences between the 10m and gradient level values, and all storms had differences

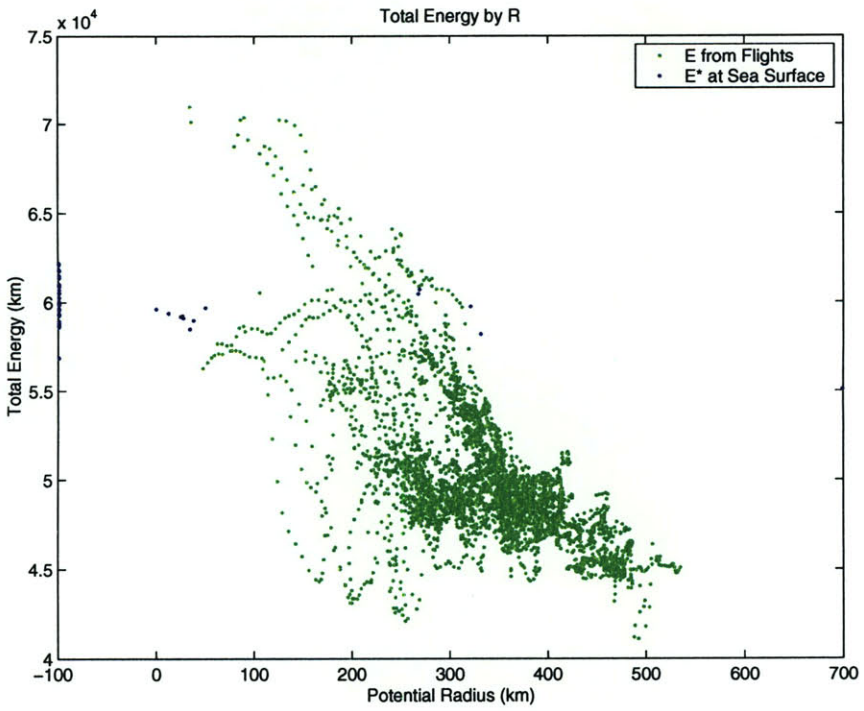

Figure 9-13: Flight Level E values vs. R for Mitch

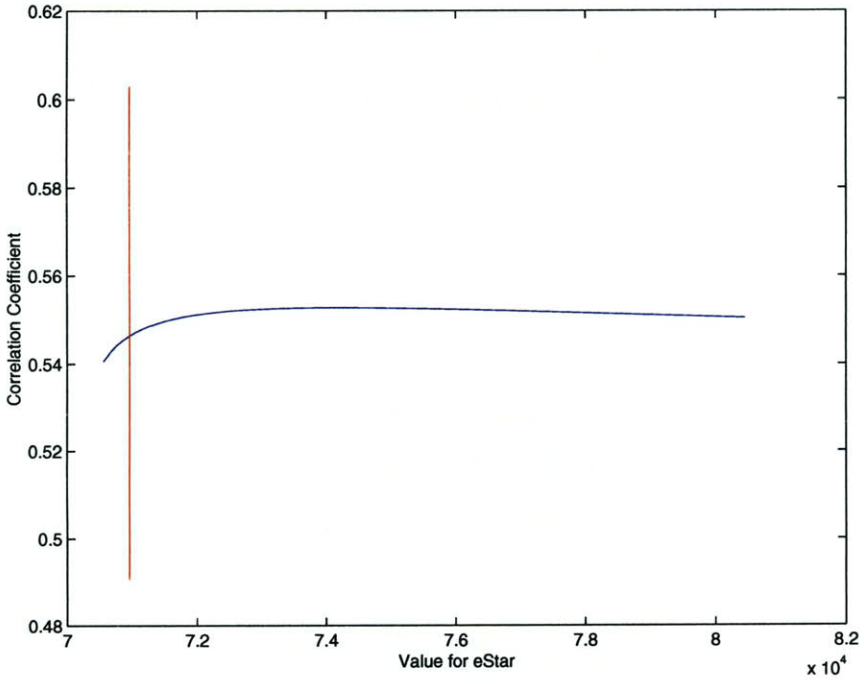

Figure 9-14: E* vs. Correlation Coefficient for Mitch

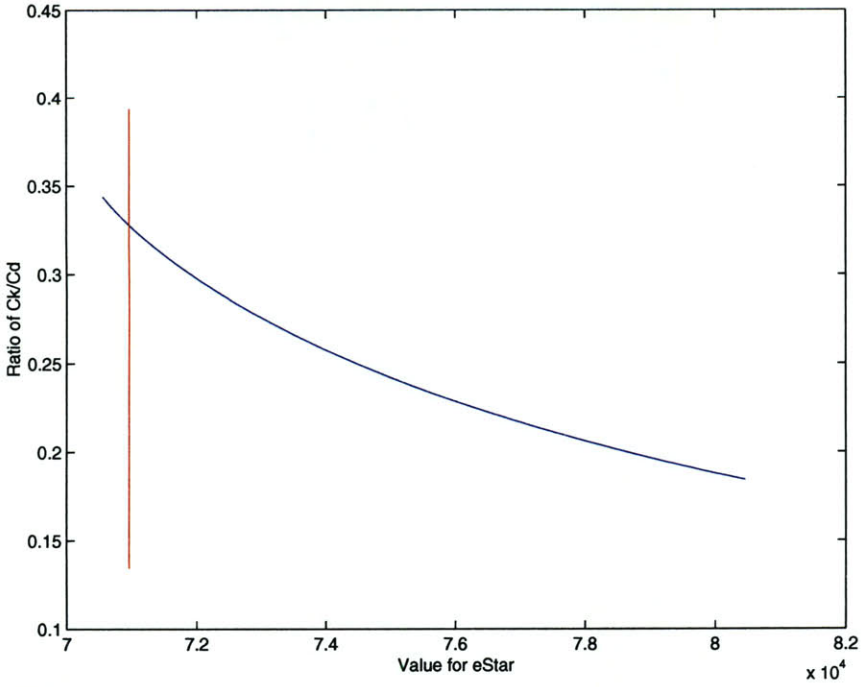

Figure 9-15: E* vs. Ratio of C_k/C_d for Mitch

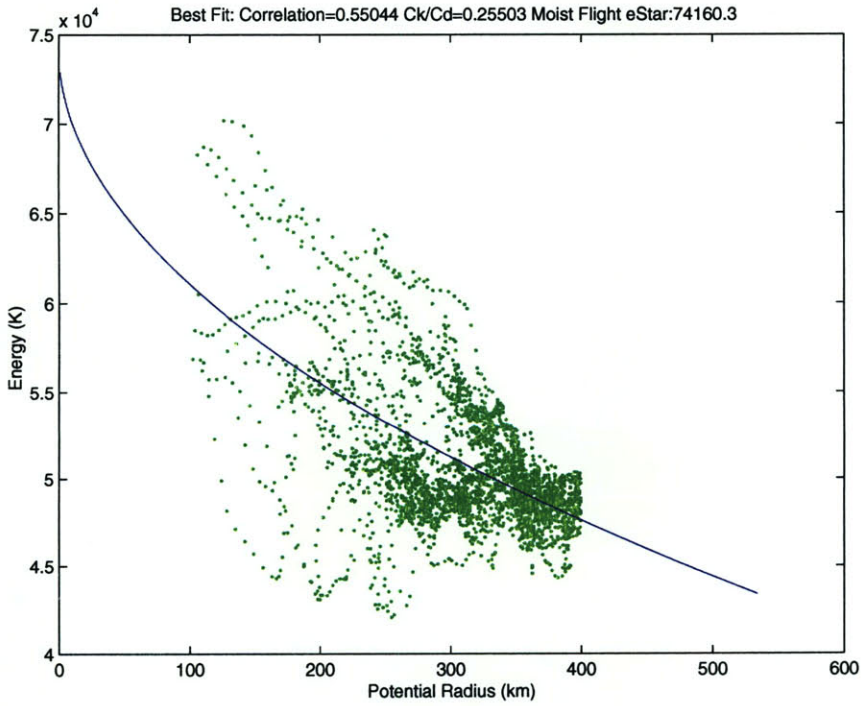

Figure 9-16: Best fit to observations for E for Mitch

Storm	Budget C_d	Budget C_k	Budget Ratio	Curve Fit Ratio
Floyd (10m)	0.0027	0.0009	0.33	0.42
Floyd (Gradient)	0.0022	0.0005	0.23	0.42
Georges (10m)	0.0028	0.0010	0.35	0.54
Georges (Gradient)	0.0012	0.0005	0.41	0.54
Mitch	0.0043	0.0008	0.19	0.25
Mitch (Gradient)	0.0022	0.00038	0.17	0.25

Table 9.2: Summary of C_k/C_d Ratio Calculations

Storm	Budget C_d	Budget $C_k withEddy$	Budget Ratio	Curve Fit Ratio
Floyd (10m)	0.0027	0.0029	1.07	0.42
Floyd (Gradient)	0.0022	0.0016	0.73	0.42
Georges (10m)	0.0028	0.0036	1.29	0.54
Georges (Gradient)	0.0012	0.0020	1.67	0.54

Table 9.3: Summary of C_k/C_d Ratio Calculations with Eddy Term Included

between the budget values and the flight level values. While there is some scatter in the values, they fall in a range between 0.17 and 0.54, i.e. always less than 1.0, with the lowest values observed in Mitch. Both these budget and ratio forms, though, do not include the eddy heat fluxes.

Calculations including the eddy fluxes in the budget ratio are shown in table 9.3. The curve-fit ratio values are provided for comparison; these do not include the eddy flux term, but would be expected to change similarly if it were added. We can see that the budget ratios for Floyd and Georges are much closer to 1.0; the Georges gradient case seems to have a relatively small value for C_d, which leads to a high ratio value. The ratios for Mitch are not included, as the eddy flux term was negative. This result for Mitch is probably related to the weakening it was undergoing at the time of these observations. The average budgeted ratio of C_k/C_d for Floyd and Georges is 1.19. As the eddy fluxes were calculated above the top of the boundary layer, their values at the top of the boundary layer are probably a bit smaller; use of these adjusted values would lead to a ratio of around unity.

Chapter 10

Conclusions

The values of the drag coefficient and heat transfer coefficient show behavior that is in line with previous observational and theoretical studies. That is, the drag coefficient increases (at least for a while) with wind speed, and the enthalpy transfer coefficient also has larger values than at lower windspeeds. Eddy fluxes were also shown to be a significant effect in determining the value of C_k.

The values for C_d and C_k were calculated both at the 10m level and at the gradient wind level. The 10m calculations are for comparison with literature values; the gradient level calculations are useful in numerical modeling studies where 10m winds are not computed.

10.1 Drag Coefficient

The 10m drag coefficient results are quite consistent between all three storms, if the surface wind speed adjustment is made for the case of Mitch. Values are in the range of 0.0026 to 0.0030, which is in good agreement with the existing literature. The gradient level values of the drag coefficient for all three storms have a mean of 0.0019 and a mean standard deviation of 0.0010. These cases represent the highest wind speeds for which the coefficients have been calculated in the existing literature. This shows that the value of C_d does not continue to increase with windspeed much beyond hurricane force. Previous studies have shown that the cause of the increase of the drag coefficient with windspeed is the interaction with growing, young waves. With very strong winds, wave height may not continue to increase,

rather the waves may be smoothed and flattened by the intensity of the winds. This could be a mechanism that prevents the drag from increasing further.

10.2 Heat Flux Coefficient

Evaluation of the flight level data showed a significant eddy flux of energy and entropy for Floyd and Georges. The values were smaller and negative for Mitch. This indicates that the smaller scale updrafts and downdrafts are important for these budgets, as well as the large scale, steady flow.

The values of C_k with eddy flux included vary somewhat between storms. For the 10m values, the range is from 0.0029 for Floyd and 0.0036 for Georges. The values produced by budgets of enthalpy and entropy give very similar values in these cases. The gradient level values for C_k are also consistent between the storms, and are around 60% of the magnitude of the 10m values. They range from about 0.0016 for Floyd to 0.0020 for Georges.

Mitch was not an ideal case for this work because it had passed its peak intensity by the time of the observations and had begun to weaken.

10.3 Ratio C_k/C_d

The mean ratio from the budget calculations is 0.29 ± 0.09 and the mean ratio from the flight-level (plus boundary layer ratio for Floyd) data is 0.46 ± 0.16. In aggregate from all of the methods of calculating C_k/C_d without eddy flux, we find an average that is below 0.5.

When the eddy fluxes of energy and entropy are included in the estimation of the ratio, an average value of 1.19 was obtained for Floyd and Georges. This is in line with the values predicted in Emanuel (1995a), which suggests that C_k/C_d should be between 1.2-1.5 (without the effect of dissipative heating).

10.4 Summary

The budget calculations in this study have shown that the 10m drag coefficient has a value of 0.0026 to 0.0030 for windspeeds in the 40-60 ms^{-1} range. They have also shown that the 10m enthalpy transfer coefficient ranges from 0.0029 to 0.0036 in these conditions for Floyd and Georges, though with much smaller values for Mitch. Gradient level values are smaller, as expected. For C_d, the gradient level value is 0.0019 ± 0.0010 and for C_k, it is 0.0016 for Floyd and 0.0020 for Georges. These values indicate that the ratio of C_k/C_d is close to or slightly larger than unity for an intense hurricane.

Bibliography

M. Bister and K.A. Emanuel. Dissipative Heating and Hurricane Intensity. *Meteor. Atmos. Physics*, 65:233–240, 1997.

M. Black. Mission Summary 980919I1 Hurricane Georges. Technical report, NOAA, Atlantic Oceanographic and Meteorological Laboratory, Hurricane Research Division, Miami, FL, 1998a.

M. Black. Mission Summary 981027I1 Hurricane Mitch. Technical report, NOAA, Atlantic Oceanographic and Meteorological Laboratory, Hurricane Research Division, Miami, FL, 1998b.

M. Black. Mission Summary 990913H Hurricane Floyd . Technical report, NOAA, Atlantic Oceanographic and Meteorological Laboratory, Hurricane Research Division, Miami, FL, 1999.

D.R. Caldwell and W.P. Elliott. Surface Stresses Produced by Rainfall. *J. Phys. Oceanogr.*, 1(2):145–148, 1971.

K.A. Emanuel. An Air-Sea Interaction Theory for Tropical Cyclones. Part I: Steady State Maintenance . *J. of the Atmospheric Sciences*, 43:585–604, 1986.

K.A. Emanuel. The Maximum Intensity of Hurricanes . *J. of the Atmospheric Sciences*, 45:1143–1155, 1988.

K.A. Emanuel. *Atmospheric Convection.* Oxford University Press, 1994.

K.A. Emanuel. Sensitivity of Tropical Cyclones to Surface Exchange Coefficients and a Revised Steady-State Model Incorporating Eye Dynamics . *J. of the Atmospheric Sciences*, 52:3969–3976, 1995a.

K.A. Emanuel. The Behavior of a Simple Hurricane Model Using a Convective Scheme Based on Subcloud-Layer Entropy Equilibrium. *J. of the Atmospheric Sciences*, 52:3960–3968, 1995b.

K.A. Emanuel. Some Aspects of Hurricane Inner-Core Dynamics and Energetics. *J. of the Atmospheric Sciences*, 54:1014–1026, 1997.

C.W. Fairall, E.F. Bradley, D.P. Rogers, J.B. Edson, and G.S. Young. Bulk Parameterization of air-sea fluxes for Tropical Ocean-Global Atmosphere Coupled-Ocean Atmosphere Response Experiment. *J. Geophys. Res.*, 101:3747–3764, 1996.

G.L. Geernaert, S.E. Larson, and F. Hansen. Measurements of the Wind Stress, Heat Flux, and Turbulence Intensity During Storm Conditions over the North Sea. *J. Geophys. Res.*, 92(12):13127–13139, 1987.

H.F. Hawkins and D. T. Rubsam. Hurricane Hilda, 1964: II. Structure and Budgets of the Hurricane on October 1, 1964 . *Monthly Weather Review*, 96:617–636, 1968.

T. F. Hock and J. L. Franklin. The NCAR GPS Dropwindsonde . *Bulletin of the American Meteorological Society*, 80:407–420, 1999.

J.R. Holton. *Introduction to Dynamic Meteorology.* AcademicPress, 1992.

J.V. Iribarne and W.L. Godson. *Atmospheric Thermodynamics.* D. Reidel Pub. Co., 1981.

V.S. Korolev, S.A. Petrichenko, and V.D. Putov. Heat and Moisture Exchange between the Ocean and Atmosphere in Tropical Storms Tess and Skip. *Meteorologiya i Gidrologiya*, 2:108–111, 1990.

T.N. Krishnamurti and L. Bounoua. *An Introduction to Numerical Weather Prediction Techniques.* CRC Press, 1999.

W.G. Large and S. Pond. Open Ocean Momentum Flux Measurements in Moderate to Strong Winds. *J. Phys. Oceanogr.*, 11:324–336, 1981.

W.G. Large and S. Pond. Sensible and Latent Heat Flux Measurements over the Ocean. *J. Phys. Oceanogr.*, 12:464–482, 1982.

W.T. Liu, K.B. Katsaros, and J.A. Businger. Bulk Parameterization of Air-Sea Exchanges of Heat and Water Vapor Including the Molecular Constraints at the Interface. *J. of the Atmospheric Sciences*, 36:1722–1735, 1979.

K. Ooyama. Numerical simulation of the life cycle of tropical cyclones . *J. of the Atmospheric Sciences*, 26:3–40, 1969.

H. Riehl and J. Malkus. Some Aspects of Hurricane Daisy, 1958 . *Tellus*, 13:181–213, 1961.

L. R. Schade. *The Ocean's Effect on Hurricane Intensity.* PhD thesis, Massachusetts Institute of Technology, 1994.

S.D. Smith and E.G. Banke. Variation of the Sea Surface Drag Coefficient with Wind Speed. *Q.J.R. Meteorol. Soc*, 101:665–673, 1975.

S.D. Smith. Wind Stress and Heat Flux over the Ocean in Gale Force Winds. *J. Phys. Oceanogr.*, 10:709–726, 1980.

J. Wu. Wind-Stress Coefficients over Sea Surface near Neutral Conditions – A Revisit. *J. Phys. Oceanogr.*, 10:727–740, 1980.